Front. Energy 2025, 19(5): 642–669
https://doi.org/10.1007/s11708-025-1004-6

REVIEW ARTICLE

Current advances and performance enhancement of single atom M-N-C catalysts for PEMFCs

Yanhong Lin[1], Wenjun Li[1], Zeyu Wang[1], Yun Zheng[3], Yining Zhang (✉)[2], Xiaogang Fu (✉)[1]

1 State Key Laboratory of Solidification Processing, Atomic Control and Catalysis Engineering Laboratory, School of Materials Science and Engineering, Northwestern Polytechnical University, Xi'an, 710072, China
2 Yulin Innovation Institute of Clean Energy, Yulin 719000, China
3 Institute of New Energy Materials and Engineering, School of Materials Science and Engineering, Fuzhou University, Fuzhou 350108, China

Abstract Single-atom transition metal-nitrogen-doped carbons (SA M-N-Cs) catalysts are promising alternatives to platinum-based catalysts for the oxygen reduction reaction (ORR) in proton exchange membrane fuel cells (PEMFCs). However, enhancing their performance for practical applications remains a significant challenge. This review summarizes recent advances in enhancing the intrinsic activity of SA M-N-C catalysts through various strategies, such as tuning the coordination environment and local structure of central metal atoms, heteroatom doping, and the creation of dual-/multi metal sites. Additionally, it discusses methods to increase the density of M-N_x active sites, including chelation, defect capture, cascade anchoring, spatial confinement, porous structure design, and secondary doping. Finally, it outlines future directions for developing highly active and stable SA M-N-C catalysts, providing a comprehensive framework for the design of advanced catalysts.

Keywords single atom catalysts, metal-nitrogen-carbon, oxygen reduction reaction (ORR), catalytic performance, proton exchange membrane fuel cells (PEMFCs)

1 Introduction

The advancement of science and technology, combined with the rapid pace of societal development, has resulted in a significant increase in energy demand. This, in turn, has led to a rising dependence on non-renewable energy sources. Consequently, there is an urgent need for scientists to expeditiously investigate novel energy technologies that can replace non-renewable energy sources, particularly in the growing electric vehicle market [1]. In this context, proton exchange membrane fuel cells (PEMFCs) have gained significant attention in recent years because of their theoretical utilization efficiency of up to 100% [2]. Nevertheless, the commercialization process of PEMFCs is hindered by the high cost and limited activity of catalysts [3]. Consequently, the development of high-efficiency, low-cost non-platinum group metal (non-PGM) single-atom catalysts to enhance the performance of PEMFC represents a key research challenge and a highly promising avenue of investigation [4,5].

Previous studies have shown that during the oxygen reduction reaction (ORR), O_2 adsorbed at the active site undergoes either a 4-electron or a 2-electron process (which exists in either acidic or basic electrolytes). While the 2-electron process produces a peroxide, which can undermine both stability and activity [6], the 4-electron process is more efficient. Therefore, it is crucial to precisely design the active site in the catalyst to enable the ORR to proceed efficiently along the 4-electron route [7]. M-N_x, identified as active sites in non-PGM monatomic catalysts [8], have shown potential for improving both stability and activity. Further investigation into M-N_x sites in monatomic catalysts is necessary to enhance their performance [9].

Compared to platinum group metal (PGM) catalysts, non-PGM single-atom catalysts are considered to be the most promising catalysts not only due to their atomically dispersed M-N_x active sites [10], which result in extremely high metal atom utilization efficiency and enhance ORR efficiency, but also due to their abundant sources and inexpensive costs. However, challenges

Received Jan. 20, 2025; accepted Mar. 17, 2025; online Apr. 30, 2025
Correspondences: Yining Zhang, zhangyn@dnlyl.ac.cn;
Xiaogang Fu, xiaogangfu@nwpu.edu.cn

remain in applying non-PGM single-atom catalysts to PEMFCs [11–13]. One major issue is the stability problem of these catalysts. Due to the highly dispersed single atoms on the surface of catalysts, they are susceptible to aggregation, leading to the degradation of catalyst performance [14]. Additionally, improving the activity of single-atom catalysts to make them more effective in PEMFC remains the focus of current research.

Iron-based catalysts, in particular, exhibit high catalytic activity in PEMFCs, and their performance can be optimized by adjusting coordination structures and electronic states [15–17]. The relatively low cost of iron-based catalysts also offers promising prospects for a broader application [18–20]. Other non-Pt group metals can similarly serve as the central metal atom in M-N_x catalysts. Therefore, an in-depth study on enhancing the activity of non-PGM single-atom catalysts is crucial for accomplishing the US Department of Energy's goal of reducing fuel cell costs by improving their efficiency and expanding their application range [21].

This review summarizes recent advancements in enhancing the activity of M-N-C catalysts in PEMFCs, including enhancing the intrinsic activity of M-N-C catalysts and increasing the density of active sites. It focuses on strategies to enhance intrinsic activity of catalysts, such as tuning the coordination structure of the central atom, doping of heteroatoms, constructing dual- or multi-metal sites, and modulating carbon materials. It also explores strategies for increasing the density of active sites, including chelation, adsorption, and other methods to strengthen the M-N bond and prevent metal aggregation. The objective of these strategies is to reduce the formation of metal aggregates and thus increase the active site density. Additionally, it discusses secondary atom doping, spatial confinement, porous structure design, cascade anchoring as strategies to further increase active site density and promote catalysts activity. Finally, it summarizes the current state of M-N-C catalysts and provides an outlook for future developments.

2 Acid ORR mechanism

The ORR of a PEMFC occurs at the cathode under acidic conditions, as shown schematically in Fig. 1(a) [22]. At the cathode, oxygen from the air reacts with protons produced at the anode and traveled through the proton exchange membrane to the cathode. Electrons, transported through the external circuit, combine with the protons and oxygen to produce water. In general, the ORR is highly dependent on the pH of the electrolyte [23]. This section focuses on ORR reactions under acidic conditions [24].

It is well known that ORR reactions are kinetically slow due to their different reaction pathways and the involvement of many intermediates along the way to the reaction. The reactions involved in ORR are illustrated in Fig. 1(b) [25]: ① the direct four-electron pathway, where O_2 is reduced to H_2O, and ② the indirect two-electron pathway, in which O_2 is first reduced to hydrogen peroxide (H_2O_2) and then further reduced to H_2O, with H_2O_2 acting as an intermediate. In addition, the H_2O_2 intermediate can either be reversibly decomposed to O_2 or directly diffused into the solution (k is the reaction rate constant for the different reactions) [26,27].

(1) Four electronic pathways

$$O_2 + 4H^+ + 4e^- \rightarrow 4H_2O,\ E_0=1.229\ V \quad (1)$$

(2) Two electronic pathways

$$O_2 + 2H^+ + 2e^- \rightarrow H_2O_2,\ E_0=0.670\ V \quad (2)$$

$$H_2O_2 + 2H^+ + 2e^- \rightarrow 2H_2O,\ E_0=1.770\ V \quad (3)$$

The process of both the four-electron and two-electron pathways involves multiple steps.

(3) Four electronic pathways

$$O_2 + * \rightarrow O_2* \quad (4)$$

$$O_2* + H^+ + e^- \rightarrow OOH* \quad (5)$$

$$OOH* + H^+ + e^- \rightarrow O* + H_2O \quad (6)$$

$$O* + H^+ + e^- \rightarrow OH* \quad (7)$$

$$OH* + H^+ + e^- \rightarrow H_2O \quad (8)$$

(4) Two electronic pathways

$$O_2 + * \rightarrow O_2* \quad (9)$$

$$O_2* + 2H^+ + 2e^- \rightarrow H_2O_2 \quad (10)$$

$$H_2O_2 + 2H^+ + 2e^- \rightarrow 2H_2O \quad (11)$$

In the above equations, "*" represents the active state, indicating that ORR activity is closely related to the strength of adsorption/desorption between active sites and intermediates. Yeager proposed three modes of adsorption of oxygen molecules, as shown in Fig. 1(c) [28]. These include:

The Griffith model (side-based model): Oxygen molecules form bonds with atoms parallel to the electrode surface, weakening the O−O bond and facilitating the four-electron pathway.

The Pauling model (End-based model): Oxygen molecules form a direct bond with one of their oxygen atoms to the active site on the electrode surface. In this model, oxygen molecules adsorb perpendicularly to the electrode surface in end-pairs, with the unbonded oxygen atom pointing away from the electrode. This model is not favorable for O−O bond breaking, often leading to the two-electron pathway.

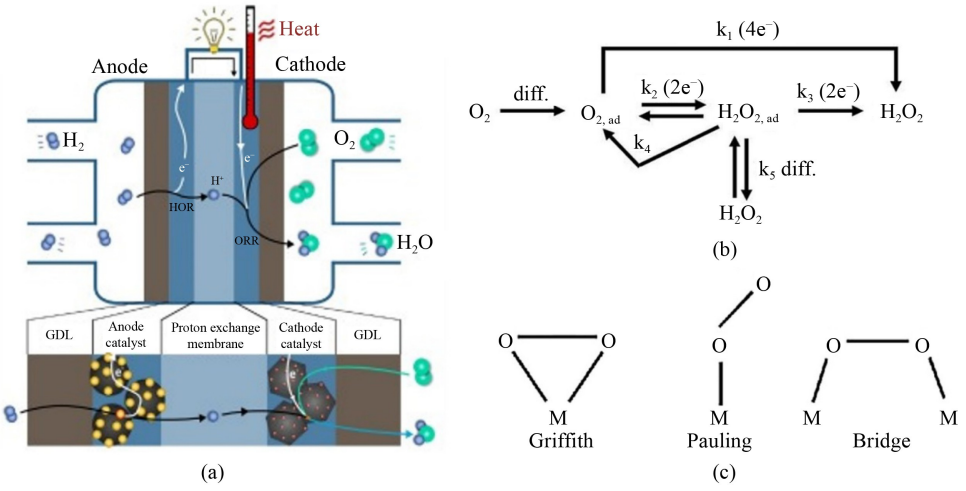

Fig. 1 Mechanistic illustration of ORR in PEMFC.

(a) Schematic of ORR for PEMFC (adapted with permission from Kim et al. [22], copyright 2021, Elsevier); (b) reaction pathways involved in ORR (adapted with permission from Pang et al. [25], copyright 2023, John Wiley and Sons); (c) oxygen adsorption pattern on catalyst surface (adapted with permission from Liu et al. [28], copyright 2019, Springer Nature).

The Bridge model (Yeagar model): Two oxygen atoms in the oxygen molecule form bonds with two different atoms or active sites on the surface of the electrode simultaneously, contributing to O−O bond breaking and facilitating the four-electron pathway [29].

The ORR mechanism is directly relevant to the design of M-N-C catalysts, which are widely studied for their potential to replace platinum-based catalysts in PEMFCs. M-N-C catalysts, featuring metal-nitrogen-carbon active sites, selectively promote the four-electron pathway by optimizing the adsorption/desorption of intermediates. For example, Fe-N_4 sites in M-N-C catalysts exhibit strong binding with OOH* and OH* intermediates, facilitating their reduction to H_2O. Additionally, the electronic structure of M-N-C sites can be tuned to weaken O−O bonds, further enhancing the four-electron pathway. By integrating advanced characterization techniques and theoretical calculations, researchers can better understand how M-N-C catalysts stabilize intermediates and improve ORR performance under acidic conditions. This understanding is crucial for developing high-performance M-N-C catalysts for practical PEMFC applications. Therefore, an in-depth understanding of the ORR mechanism is essential for the rational design of M-N-C catalysts.

3 Strategies to enhance the intrinsic activity of M-N-C

The activity of M-N-C catalysts is closely related to the intrinsic activity of their active sites, which in turn determines the adsorption/desorption energies of intermediates of the ORR reaction pathway at the active sites. These energy interactions directly influence the rate of the ORR and, consequently, the overall catalyst activity [30]. This review summarizes the common approaches to modifying the electronic configuration of the active site, for example, tuning the coordination condition of the central atom, doping of heteroatom, construction of dual/multi-metallic sites, and modulation of carbon materials, with particular emphasis on coordination engineering of the central atom.

3.1 Tuning the coordination structure of central atom

In the 4-electron process of ORR, the intermediate product is transformed into H_2O through a protonation step via adsorption at the active site. However, the exact mechanism of ORR remains unclear [31]. Based on the rate of hydrogen-oxygen binding, it has been proposed that the O* or OH* species formed after the O = O bond is broken, are adsorbed on the metal site and adjacent N or C atoms, respectively. Water is then produced through several different protonation steps, with the formation of H_2O_2 or H_2O depending on the breaking of the O=O bond in the OOH* [32,33]. Therefore, the adsorption of intermediates on the active site is crucial for the reaction [24,34].

However, the strength of adsorption should be neither too strong nor too weak at the M-N_x sites. The strength of adsorption of intermediates varies with different central metal atoms, affecting the overall ORR activity. For instance, Fe exhibits a significantly stronger adsorption capacity compared to Co [35]. Consequently, tuning the coordination structure of the central atom is important for enhancing the intrinsic activity of M-N-C catalysts [36–39].

3.1.1 Altering the number of N ligands

Density functional theory (DFT) calculations show that there are five possible coordination numbers for N atoms for M-N-C electrocatalysts, with X = 1–5. Altering the coordination number significantly impacts the charge distribution of the central metal atom, especially the d-band electrons [40], which in turn influences the intrinsic activity of M-N-C catalysts. Many studies have explored this relationship, offering different viewpoints [41]. For example, theoretical calculations suggest that the activity of FeN_4 in the ORR process follows the order of 4 > 3 > 2 > 1 > 5 [42,43]. Consequently, recent studies have focused heavily on M-N_4 sites [32,44,45].

Among the various M-N_4 sites (M = Fe, Co, Mn, Cu, Ni, Zn, etc.), FeN_4 has been extensively studied due to its superior ORR activity. FeN_4 exhibits the lowest free energy in the rate-determining step (RDS) of the ORR process [46], making it more efficient than other metal atoms in most reports. In a study by Li et al., Fe-N-C catalysts with different Fe-N coordination numbers were prepared by controlling the heating temperature (Fig. 2(a)) [47]. The formation energies of the synthesized catalysts showed an "inverted volcano" relationship with the x-number of FeN_x, and ORR activities showed a "volcano" relationship with x. The study demonstrated that FeN_4 (FeNC-1000) exhibited the best ORR and PEMFC performance due to its low formation energy.

The effect of the number of N ligands on the activity of CoN_4 was investigated by Yang et al. with DFT calculations verifying the effect of different structures of CoN_x on the ORR activity. As shown in Fig. 2(b) [48], the key factor affecting the ORR activity is the adsorption mode of O*, and the adsorption energies of different structures induced by different adsorption modes of O* consistent with the trend of the U^{onset} change. This implies that CoN_4 is the best active center with the highest activity, confirming that that M-N_4 molecules embedded in the carbon skeleton are the most active for ORR.

However, previous studies have shown that the superior performance of FeN_2 is due to the weaker adsorption of $*O_2$ and *OH intermediates at active sites, which can be easily desorb to generate H_2O [49]. Qi and colleagues demonstrated that the activity of bi-FeN_2 is much higher than its isolated state by embedding the bi-FeN_2 molecules in graphene. This enhancement is

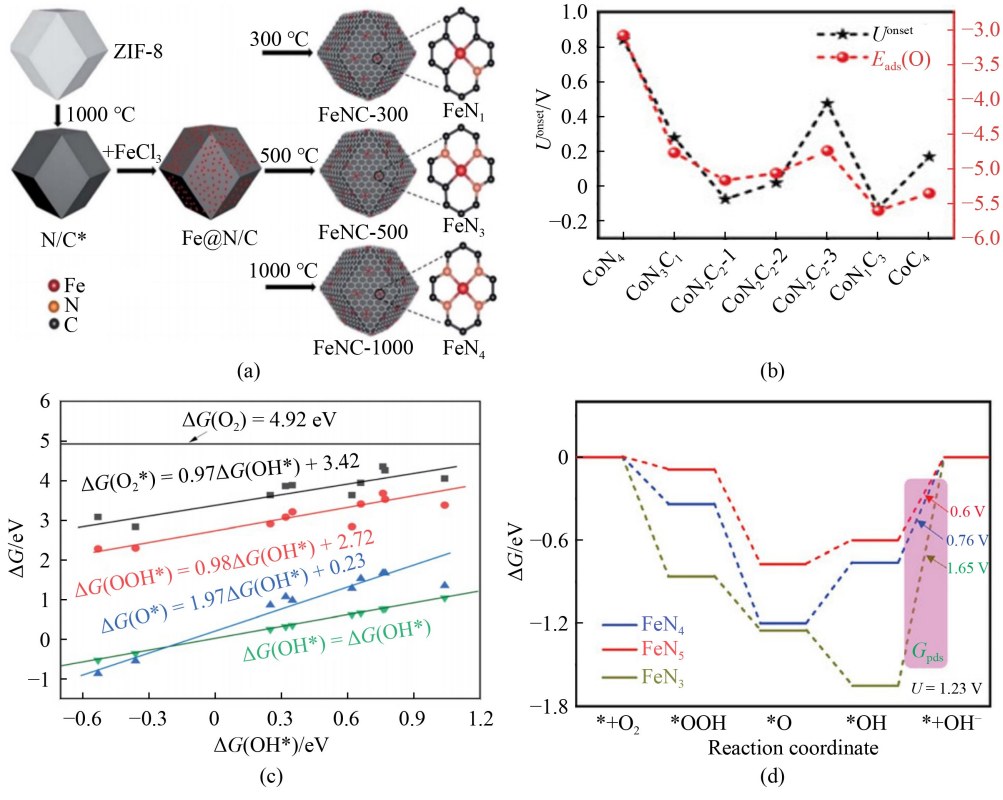

Fig. 2 Structural schematic and electronic structure analysis of catalysts with varied nitrogen ligands.
(a) Schematic representation of Fe-NC formed at different temperatures with different amounts of nitrogen ligands (adapted with permission from Wang et al. [47], copyright 2024, Elsevier); b) relationship between onset voltage and oxygen atom adsorption energy on $CoN_4@_xC_x$ (adapted with permission from Yang et al. [48], copyright 2020, John Wiley and Sons); (c) comparison of free energies of oxygenated intermediates in the active site, where *OH is the descriptor (adapted with permission from Qi et al. [50], copyright 2016, Royal Society of Chemistry); (d) Gibbs free energy diagram for ORR over different model catalysts (adapted from Wang et al. [51] under the terms of CC BY-NC-ND license).

attributed to the bridge adsorption structure of oxygen-containing intermediates at the active site, with the adsorption trend following $H_2O < O_2 < OOH < OH < O$ (Fig. 2(c)) [50]. Additionally, the activity of isolated FeN_4 is much greater than that of other isolated FeN_x configurations.

In contrast, a recent study showed that FeN_5 site has higher ORR activity compared to FeN_4 and FeN_3 sites. To prove this, the researchers calculated the free energies for FeN_5, FeN_4, and FeN_3 site models for the basic steps of the ORR process (Fig. 2(d)) [51]. DFT results showed that the ORR reactivity follows the order of $FeN_5 > FeN_3 > FeN_4$. In addition, FeN_5 also has higher power density and durability, which suggests that it has superior intrinsic activity. Liu's group also developed a Fe-N/C ORR catalyst with FeN_3 sites dispersed in a multiscale porous carbon framework (eFe-N_3/PCF) by combining a self-assembly process and high-temperature metal etching effect, which achieved onset and half-wave potentials of 1.090 and 0.934 V, respectively [52].

Although FeN_x catalysts synthesized by different strategies and with different numbers of N ligands have different ORR activities, FeN_4 still generally exhibits the highest ORR activity, compared to other ligand numbers, as predicted by DFT calculations.

M-N_5 refers to the active site where the M-N_4 site in the same plane is coordinated to an additional N atom in another plane, forming an axial five-coordinated site [25,53–55]. Liu et al. reported a Fe-N_5/C@G SAC catalyst with FeN_5 sites in monolayer graphene, which achieved a current density of up to 1.65 mA/cm^2 at 0.88 V potential, outperforming FeN_4 and Pt/C catalysts [56]. This further corroborates DFT calculations regarding the active coordination structure of FeN_x (x = 1–5) embedded in a carbon six-membered ring. Xia et al. designed a FePc/NGM catalyst with axial interactions of FeN_4 and NGM graphene, incorporating FeN_5 sites, which has an excellent ORR activity [57].

While M-N_5 sites have higher ORR activity due to their ability to lower the reaction barriers [58], finding a simple and effective method to obtain M-N_5 active sites with precise coordination numbers remains a significant challenge. Axial coordination improves activity compared to the traditional M-N_4 planar configuration because the central metal atom can accept electrons from ligands [59]. This interaction, combined with the planar coordination environment, alters the electronic structure of the active site, optimizing the adsorption energy of intermediates [60]. As a result, catalysts with axially coordinated M-N_5 active sites exhibit superior performance.

3.1.2 Strain effects of M-N

In addition to tuning the number of coordination sites in the metal center, the ORR activity can also be improved by adjusting the distance between the metal and coordination atoms, often referred to as modifying the M-N bond lengths. Li and colleagues reported a study in which solid iron oxide precursors were directly transformed into single-metal-site catalysts. They also predicted the structural formation of these catalysts at different temperatures and found that changes in Fe-N bonding affected O_2 adsorption and the subsequent O=O bond-breaking process. Specifically, a smaller Fe-N bond (< 2%) shortening led to changes in its electronic structure, promoting O_2 adsorption at FeN_4 sites. In contrast, a more significant Fe-N bond change (> 5%) negatively impacted the ORR activity. These findings corroborate theoretical calculations that suggest the ORR activity improves at higher temperatures, likely due to a slight contraction of the Fe-N bond (Fig. 3(a)) [61].

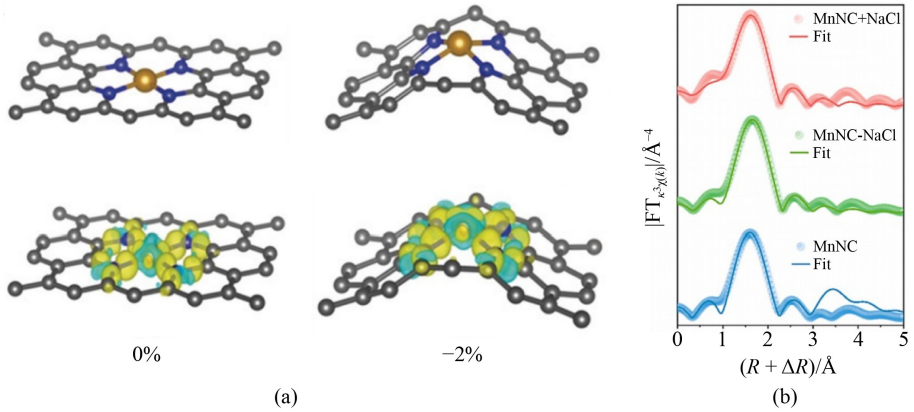

Fig. 3 Structural analysis of strain effects on M-N bonding in catalytic active sites.

(a) Schematic geometry and charge distribution of the normal Fe-N bond and the 2% contracted FeN_4 site (yellow, gray, and blue spheres representing Fe, C, and N atoms, respectively) (adapted with permission from Li et al. [61], copyright 2019, John Wiley and Sons); (b) EXAFS spectral function fitting curves of Mn-NC under the influence of NaCl (adapted with permission from Wen et al. [62], copyright 2023, Elsevier).

In addition to temperature control, the M-N bond length and the ORR activity can be regulated using the template methods. A recent research demonstrated that Mn-N-C catalysts obtained from precursors grown on NaCl templates were further optimized by controlling the secondary calcination temperature (Fig. 3(b)) [62]. The Mn-N-C catalysts grown on NaCl templates had the shortest Mn-N bond lengths, which greatly promotes the adsorption and desorption of O_2 and intermediates compared to NaCl-free templates, leading to improved ORR activities. In this case, the Mn-N bond performs optimally when shortened by approximately 4%. This difference in behavior compared to Fe-N bonds highlights the influence of the electronic structures of the central metal atoms on the optimal M-N bond length. As a result, the impact of bond length on ORR activity may vary depending on the central metal atom, preventing a uniform quantitative comparison across different metals. Overall, shortening the M-N bond positively influences the adsorption of ORR intermediates, thereby enhancing the reaction rate.

3.2 Heteroatom doping

Due to the large difference in electronegativity between the central metal atom and the N atom in the M-N_x active site of M-N-C catalysts, controlling only the number of N coordination sites has a limited impact on enhancing the intrinsic activity of these catalysts. To address the insufficient intrinsic activity, many studies have proposed adding heteroatoms (such as S, P, B, etc.) to M-N-C catalysts to regulate the electronic structure of the M-N_x active site, thereby enhancing the ORR activity [63–65].

Generally speaking, doping heteroatoms with electronegativity similar to C, such as S, P, and B, can minimize the polarization between C atoms and the heteroatoms [66,67]. However, recent studies have shown that not only the type of doped heteroatoms but also the distance between the heteroatoms and the active centers plays a critical role in affecting the ORR activity [68]. For instance, a theoretical model of FeN_4 sites in graphene doped with heteroatoms at different doping distances was proposed (Fig. 4(a)) [69]. The calculations indicated that by varying the doping distance between the heteroatoms and the Fe atoms, S-, P-, and, B-doped FeN_4 sites exhibited a better ORR activity at specific positions of S1, P3, and B3, respectively, with corresponding overpotentials of 0.563, 0.573 V, respectively (Fig. 4(b)) [69]. The thermodynamic RDS for these S-, P-, and, B-doped FeN_4 sites was the *OH resolving process. These results show that both the ORR activity and the thermodynamic RDS can be altered by adjusting the doping distances in the heteroatom-doped FeN_4.

This section focuses on four main types of heteroatom doping strategies: Environmental dopant atoms, direct coordination dopant atoms, dual-doped heteroatoms, and axial fifth ligand dopant atoms.

Environmental dopant atoms are heteroatoms that are not directly bonded to the central metal atom but influence the electronic structure of the M-N_4 active site and substrate through long-range interactions, thus contribute to enhanced ORR activity.

Direct coordination dopant atoms, as the name suggests, refer to the replacement of one or more N atoms in the M-N_4 active site of the M-N-C catalysts by heteroatom, which can influence the electronic structure and thus improve the ORR activity through interactions with the M-N_4 catalyst.

Dual-doped heteroatoms involve doping two different heteroatoms into the M-N-C catalyst to jointly regulate the electronic structure of the active site M-N_4 and promote the ORR performance.

Axial fifth-ligand dopant atoms are the process of ligating the heteroatoms to the active site through axial ligand, as previously discussed. These dopants affect the electronic structure of the M-N_4 site through interactions to reduce reaction barriers for O_2 adsorption and intermediate desorption to improve ORR activity.

3.2.1 Heteroatom doping in M-N-C catalysts

Many studies have demonstrated that heteroatoms-doped M-N-C single-atom catalysts can achieve performance comparable to or even superior to that of commercial Pt/C catalysts. For example, a recent study by Liu and colleagues introduced an S-doped Fe-N-HC catalyst, named S-Fe-N-HC TDA, which had a starting potential and half-wave potential ($E_{1/2}$) of 0.90 and 0.80 V, respectively (Fig. 5(a)) [70]. Additionally, it showed remarkable stability with a cycling range of 0.6–1.0 V at 100 mV/s, losing only 21 mV after 30000 cycles. In comparison, the $E_{1/2}$ of Pt/C decreased by 58 mV, and the actual maximum output power of the PEMFC was 682.0 mW/cm^2 (Fig. 5(b)) [70]. These results highlight the potential of S-doped Fe-N-HC catalysts as a promising alternative to Pt-based catalysts.

Similarly, Sun et al. reported a series of cobalt (Co)-based single-atom catalysts with different coordination structures to elucidate the relationship between the coordination environments of the active sites of Co-based single-atom catalysts in connection with the electrocatalytic performance of the catalysts. Their study, using Co K-edge extended X-ray absorption fine structure (EXAFS) spectra, indicated that Co-S_2N_2 was the dominant structure in S-Co-N-C. The linear sweep voltammetry (LSV) curve showed that the $E_{1/2}$ of S-Co/N/C was 0.86 V, which is higher than that of Co/O/C, Co/N/C, and Co/S/C catalysts, and comparable to that of Pt/C catalysts (Figs. 5(c) and 5(d)) [71]. In addition, DFT calculations indicated that the excellent ORR activity of these catalysts was primarily due to the doping of S

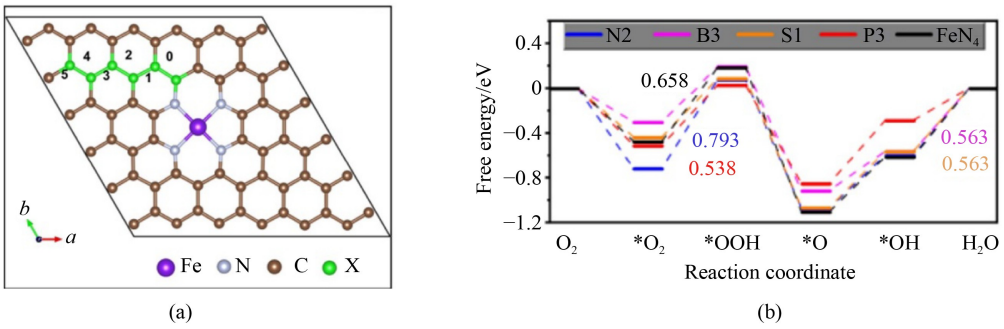

Fig. 4 Structural representations and free energy analysis of varied heteroatom doped catalysts with varied dopant configurations, (a) Schematic illustrations of 0–5 sites representing 6 different doped positions; (b) free energy levels of different heteroatoms doped FeN_4 with optimal activity (adapted with permission from Li et al. [69], copyright 2024, Springer Nature).

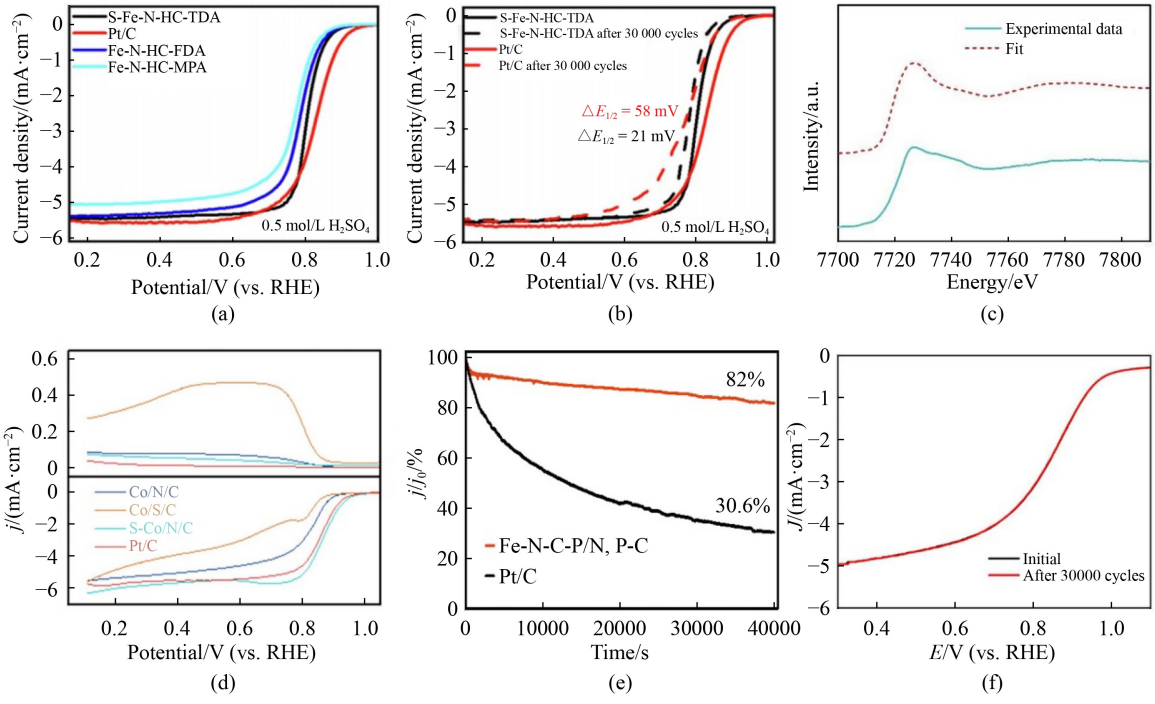

Fig. 5 Comparative performance and stability analysis of heteroatom doped catalysts.
(a) LSV curve of S-Fe-N-HC-TDA in 0.5 mol/L H_2SO_4; (b) cyclic stability of S-Fe-N-HC-TDA and Pt/C in 0.5 mol/L H_2SO_4 (adapted with permission from Liu et al. [70], copyright 2024, Elsevier); (c) experimental data and fit curves of Co K-edge EXAFS spectra for S-Co/N/C; (d) performance comparison between Co-based catalysts and commercial Pt/C (adapted with permission from Sun et al. [71], copyright 2021, American Chemical Society); (e) chronoamperometric response of Fe-N-C-P/N,P-C and Pt/C catalysts at 0.75 V (adapted with permission from Yin et al. [74], copyright 2021, American Chemical Society); (f) ORR cyclic stability of Fe-SA/PNC before and after 30000 cycles in 0.5 mol/L H_2SO_4 (adapted with permission from Xue et al [75], copyright 2023, John Wiley and Sons).

atoms, which greatly reduced the adsorption strength of intermediate *OH, facilitating the ORR process.

While P and N belong to the same group in the periodic table and have similar chemical properties, the effects produced by doping into M-N-C catalysts can be different due to the difference in their valence electrons [72,73]. Specifically, doping with P atoms leads to a redistribution of charge on the catalyst surface and negatively charges the C atoms close to the P atoms, which in turn affects the electronic structure of the whole active site. Consequently, the adsorption and desorption strength of O_2 and intermediates are altered, improving ORR performance. For example, Yin and coworkers synthesized a P-doped, N-supported edge-rich FeN_4 catalyst. This catalyst exhibited an $E_{1/2}$ of up to 0.80 V at 0.1 mol/L $HClO_4$ and a current loss of only 18% after 40000 s of continuous operation, while the current loss for Pt/C was as high as 69.6% (Fig. 5(e)) [74].

In another study, Xue et al. prepared a FeP_2N_2 catalyst, where P atoms partially replaced C atoms using a simple

chemical vapor deposition strategy. This catalyst, named Fe-SA/PNC, exhibited excellent ORR activity under acidic conditions and remained stable after 30000 cycles in 0.5 mol/L H_2SO_4 (Fig. 5(f)) [75]. This demonstrates that doping with P atoms can significantly enhance the stability and performance of Fe-based catalysts for ORR.

3.2.2 Boron (B) doping in M-N-C catalysts

B has a lower electronegativity compared to N, and when B atoms are doped as heteroatoms in M-N-C catalysts, they disrupt the electroneutrality of the active site and make the overall positive electroneutrality around the active site, which facilitates O_2 adsorption, thereby promoting the ORR activity [76]. For example, Wang and coworkers recently reported a B-doped Fe-N-C catalyst, named Fe/B/N-C, which showed better ORR performance compared to most other M-N-C catalysts in strongly acidic electrolytes (Table 1) [65]. The LSV polarization curves show only a 23 mV change after 100000 s of constant potential timer cycling, which is much smaller than the 32 mV change observed for Pt/C (Fig. 6(a)) [65].

Table 1 Performance comparison of Fe/B/N-C with other catalysts

Catalysts	$E_{1/2}$/V (vs. RHE)	Electrolyte	Ref.
Fe/B/N-C	0.74	0.1 mol/L $HClO_4$	Wang et al. [65]
VC-MOF-Fe	0.753	H_2SO_4	Hu et al. [18]
Timb-Fe_5-C	0.78	0.1 mol/L $HClO_4$	Lin et al. [15]
Co-N-PCNFs	0.81	0.5 mol/L H_2SO_4	He et al. [10]

In a previous study, Guo et al. prepared a B-doped Co-N-C catalyst, and Fourier transform-extended X-ray absorption fine structure (FT-EXAFS) spectra clearly showed two distinct characteristic peaks at approximately 0.95 and 1.5 Å. These peaks might be attributed to the Co-N and Co-B bonds, respectively, implying that B atoms may partially replace N atoms and directly coordinate with Co (Fig. 6(b)) [77]. This B-doped Co-N-C catalyst has excellent performance with an $E_{1/2}$ of 0.83 V and an ultimate current density of 5.66 mA/cm^2.

3.2.3 Axial coordination and the role of heteroatoms in M-N-C catalysts

As mentioned in the previous section, the axial coordination of N atoms significantly enhances the ORR performance of M-N-C catalysts. However, axial fifth coordination is not limited to N atoms; halogen atoms such as Cl, can also coordinate to the M-N_4 active site, reducing the interaction between oxygen-containing intermediates and the active sites, thereby improving ORR performance.

Recent studies on Fe-N/C-SAC samples demonstrate the impact of axial coordination with halogen atoms. Analysis of the EXAFS spectra fitting of Fe-N/C-SAC samples, with and without Fe-Cl, shows that the fit with Fe-Cl is much better than the one without Fe-Cl, particularly at a distance range of R = 1.90–2.20 Å. This result confirms the presence of Fe-Cl (Figs. 7(a) and 7(b)) [78]. A structural model for the Fe-N/C-SAC sample was proposed based on these findings (Fig. 7(c)) [78].

In 2021, Xin et al. [78] synthesized a Fe-N-C-SAC using a melt-mediated pyrolysis strategy, with Fe-N_4Cl as the active site. Quantitative EXAFS curve fitting indicated that the coordination numbers of Fe-N and Fe-Cl were 3.6 and 1.2, respectively, which implies that the center of the Fe atom was co-coordinated by four coplanar N atoms and one axial Cl atom to form Fe-N-C-SAC with Fe-N_4Cl as the active site. This catalyst has excellent ORR activity. Similarly, Hu and colleagues [79] produced single-atom catalysts with high metal content

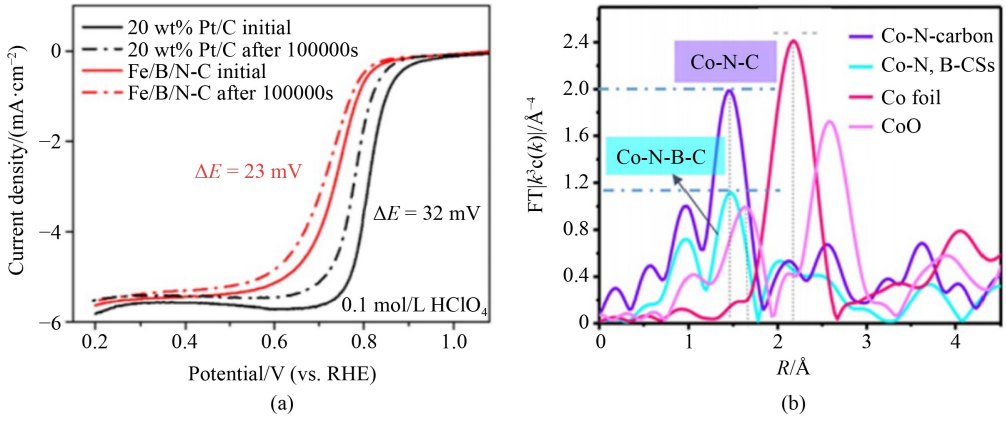

Fig. 6 Electrochemical performance and structural characterization of B-doped catalysts.
(a) Comparison of LSV performance of Fe/B/N-C and Pt/C before and after 100000s (adapted with permission from Wang et al. [65], copyright 2022, Elsevier); (b) Fourier transformed EXAFS spectra of the Co foil and Co-N, B-CSs and Co-N-carbon (adapted with permission from Guo et al. [77], copyright 2018, American Chemical Society).

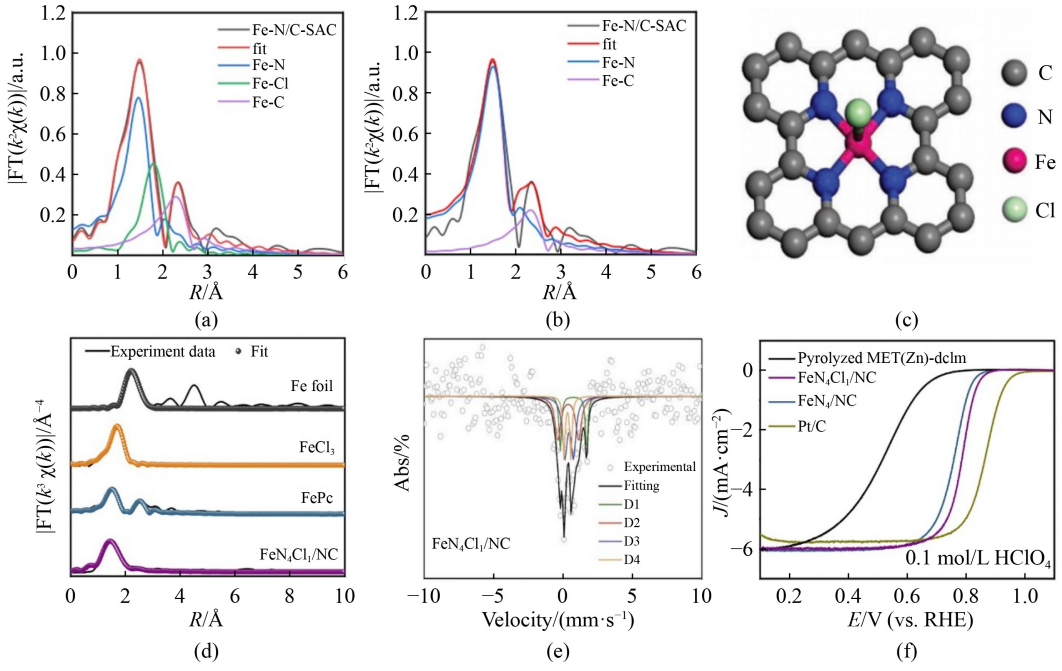

Fig. 7 Results of fitting the EXAFS spectra of Fe-N/C-SAC samples.

(a) With Fe-Cl; (b) without Fe-Cl; (c) Fe-N/C-SAC sample structure model (adapted with permission from Xin et al. [78], copyright 2021, John Wiley and Sons); (d) chemical state and coordination information for Fe SACs; (e) Mössbauer spectra of FeN_4Cl_1/NC can be fitted with four doublets; f) comparison of LSV polarization curves for various catalysts (adapted with permission from Hu et al. [79], copyright 2021, John Wiley and Sons).

(2.78 wt%), where FeN_4Cl served as the active center by pyrolysis of 4,5-dichloroimidazole-modified Zn/Fe bimetallic METs (metallotriazolyl alcohols). The EXAFS fit shows that the peak at R = 1.5Å is associated with Fe-N coordination scattering, while the peak at R = 1.71 is associated with Fe-Cl coordination scattering (Fig. 7(d)) [79]. The Mössbauer spectroscopy also proved that Cl bonded with Fe sites, where D1 belongs to the Fe-Cl species, while D2, D3, and D4 belong to the Fe-N species (Fig. 7(e)) [79]. It could be deduced that FeN_4Cl/NC was formed with FeN_4Cl as the active site, and the prepared catalysts in 0.1 mol/L $HClO_4$ had an $E_{1/2}$ of 0.79 V, which was much higher than that of the FeN_4C catalyst (Fig. 7(f)) [79]. DFT calculations also indicated that the axially coordinated Cl atoms of FeN_4 help to optimize the adsorption of *OH and make the ORR process more thermodynamically favorable.

3.2.4 Doping with electronegative atoms to optimize M-N_4 catalysts

Recent studies have shown that doping with highly electronegative O atoms can further optimize the electronic structure of M-N_4 species, improving the adsorption of intermediates and enhancing ORR performance. This approach builds on earlier research involving heteroatom doping, such as S, P, and B. For instance, Sun et al. synthesized an O-doped catalyst, O-FeN_4C-O [80]. DFT calculations revealed that O doping significantly optimizes the electronic structure of FeN_4C-O, strengthening the binding between the active site and OH intermediates, thereby enhancing ORR performance. Notably, this O-FeN_4C-O-based acidic PEMFC achieved a peak power density (PPD) of 0.88 W/cm^2.

In addition, Huo et al. synthesized a catalyst containing Mn single-atom sites, where the central Mn atom coordinated with both N and O atoms. This coordination altered the electronic structure around Mn, shifting its d-band center and generating additional unoccupied electron orbitals. These changes significantly enhanced the adsorption of intermediates, contributing to improved ORR performance [81].

Although the doping of heteroatoms in M-N-C single-atom catalysts has shown promising results and some progress has been made, there is still a need to search for new heteroatoms and establish a clearer understanding of how these elements interact with the electronic structure of the active sites. Future research should focus on accurately regulating the position and quantity of heteroatoms in the catalysts to optimize their performance and improve ORR activity.

3.3 Dual/multi-metal sites

While the ORR activity of M-N-C single-atom catalysts can be enhanced by the above strategy, the local structure of a single central metal site for optimal performance. To

address this, dual- and multi-metallic sites have emerged as a strategy to further improve ORR activity with the introduction of a second or more transition metals into the catalyst structure [82–84]. These bimetallic site single-atom catalysts can be classified into three types:

Dual-metallic isolated-site catalysts without M-M bonds: In this case, the two metal sites are not directly bonded but rather have nanoscale distances adjacent to each other, based on the coordination environments between the central metals of the active sites.

Dual-identical metal site catalysts with M-M bonds: In this case, the active sites are centered on two identical metal atoms, which are directly coordinated and bonded together.

Dual dissimilar metal site catalysts with M_1-M_2 bonds: In this case, catalysts feature two different metal atoms at the active center are bonded together different, differentiating them from the second category.

This section will explore these three types of bimetallic and the multi-metallic sites in detail [85–87].

3.3.1 Catalysts without M-M bonds

One approach to prepare catalysts with two-center metal sites without M-M bonds is to generating them *in situ* during synthesis, or by first preparing a single metal-center and then adding a precursor of the second metal [88]. Han and colleagues demonstrated this strategy by synthesizing an atomically dispersed FeCo-N-C-10 electrocatalyst obtained by adding FePc to a bimetallic organic framework (BMOF) followed by a one-step direct pyrolysis. FT-EXAFS analysis confirmed that Fe and Co did not form direct Fe-Co bonds (Figs. 8(a) and 8(b)) [89], while the coexistence of Fe-N_4 and Co-N_4 sites was established through EXAFS fitting results in the R-space of the first shell layer. The prepared FeCo-N-C-10 showed an $E_{1/2}$ of up to 0.80 V in 0.1 mol/L $HClO_4$ solution, which exhibited superior ORR activity compared to Fe-N-C or Co-N-C catalysts alone.

In another study, Kong et al. prepared an M-M bond-free electrocatalyst by a sequential synthesis method in which Fe and Cu were connected by an N bridge. The analysis of a randomly selected region indicated that the distance between two neighboring metal atoms determined by the intensity profile was close, but the distance between the two closest metal atoms (4.1 Å) was much larger than the direct bonding atomic distance (2.1 Å) (Fig. 8(c)) [90], which proves the existence of other atoms between the two metal atoms and their bonding with other atoms. The Cu wavelet transform in the Fe, Cu DAs-NC showed a maximum intensity at 4.0 $Å^{-1}$ (R = ~1.5 Å), which represents the Cu-N

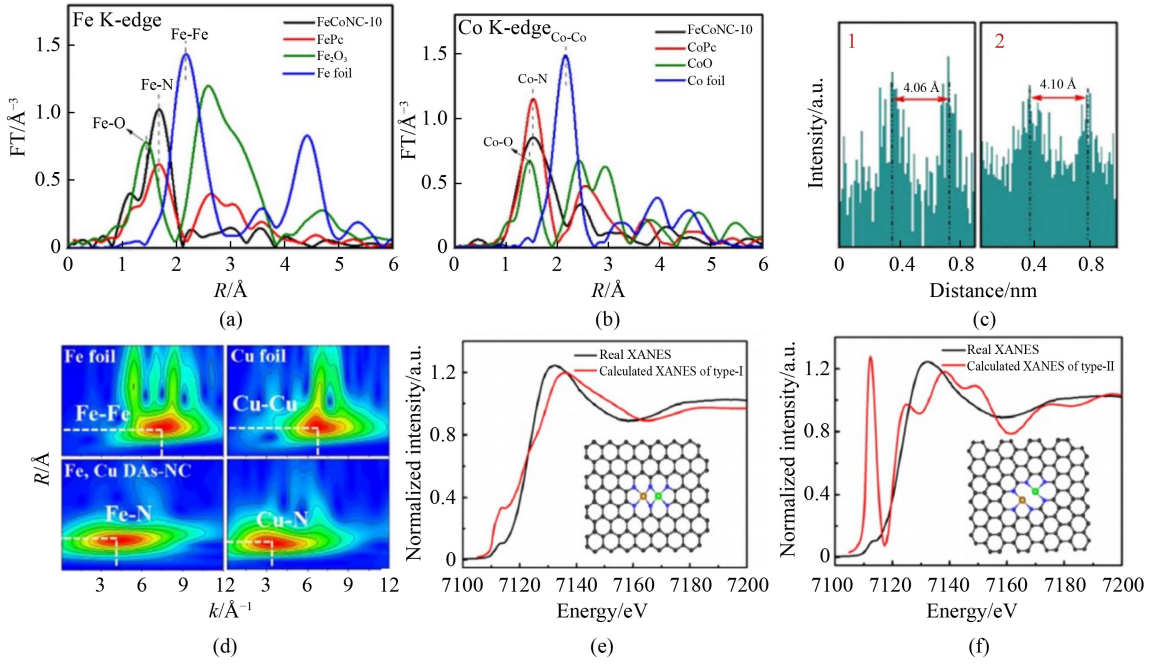

Fig. 8 X-ray absorption fine structure (XAFS) analysis of bimetallic active sites.

(a) FT-EXAFS spectra of Fe in FeCoNC-10 and standard samples; (b) FT-EXAFS spectra Co in FeCoNC-10 and standard samples (adapted with permission from Han et al. [89], copyright 2022, Elsevier); (c) line scan intensity profiles of randomly selected regions 1 and 2; (d) comparison of wavelet transformed k3-weighted EXAFS signals of Fe, Cu DAs-NC and standard samples (adapted with permission from Kong et al. [90], copyright 2023, Elsevier). (e) Fe K-edge fitting curves and structural modeling of FeNi-N_6 (type I); (f) Fe K-edge fitting curves and structural modeling of FeNi-N_6 (type II) (adapted with permission from Zhou et al. [91], copyright 2020, American Chemical Society)

coordination, and no signals corresponding to the Fe-Cu, Fe-Fe, and Cu-Cu bonds were found by comparing with the Fe, Cu DAs-NC with Fe and Cu foils, further demonstrating that the prepared catalysts do not have M-M bonds (Fig. 8(d)) [90].

3.3.2 Catalysts with M-M bonds

The above results indicate that there are one or two connecting atoms between the two metal atoms, forming a diatomic structure with in-plane bridging. In addition, Zhou et al. reported a binuclear FeNi-N_6 site embedded in a porous nitrogen-doped carbon. Similarly, the study of the coordination environments of Fe and Ni revealed that both Fe and Ni existed in the form of Fe-N and Ni-N bonds with FeNi-N_6. To clarify the specific structure of the FeNi-N_6 site, two different models were constructed and demonstrated by DFT calculations that there are two nitrogen atoms coordinated with both Fe and Ni, and each of the remaining four nitrogen atoms is coordinated with either Fe or Ni to constitute the FeNi-N_6 site (Figs. 8(e) and 8(f)) [91]. The fabricated FeNi-N_6 catalyst has an $E_{1/2}$ of 28 mV higher than that of the catalyst with single Fe-N_4 site, demonstrating the enhanced ORR activity resulting from the M-M bond.

3.3.3 Bimetallic catalysts with M-M bonds

Compared to bimetallic center-site catalysts without M-M bonds, the presence of M-M bonding in the active-site center metals can significantly affect the electronic mechanism of the center metal, thereby altering the adsorption energy of O_2. This modulation of electronic structure often results in enhanced electrocatalytic ORR activity [12,92]. For example, Wang and coworkers reported an atomically dispersed FeN_4 catalyst with Co-Co bonds, which exhibits excellent ORR performance due to the synergistic effects of Fe-N_4 and Co-Co sites. The FT-EXAFS spectra of the Co K-edge in Co_2/Fe-N@CHC showed a distinctive subminor peak at approximately 2.12 Å, which was not observed in CoPc, strongly confirming the existence of the Co-Co coordination (Fig. 9(a)) [93]. DFT calculations further demonstrated the synergistic effect of Co_2N_6 and Fe-N_4 sites, which facilitates the adsorption and desorption of *OH, the RDS in the ORR process. The Co_2/Fe-N@CHC catalyst demonstrated a peak power density of up to 232.4 mW/cm^2, higher than that of Pt/C.

3.3.4 Catalysts with dissimilar metal bonds (M_1-M_2)

Unlike bimetallic site catalysts with the same metal bonds, M_1-M_2 sites introduce more complexity into the ORR reaction. The different chemical properties of the metals lead to distinct coordination environments that can be finely tuned for higher ORR performance. Yang et al. recently reported an atomically dispersed FeCe-N doped hierarchical porous carbon catalyst, named FeCe-SAD/HPNC. Quantitative least squares EXAFS curve fitting analysis showed that the Fe-N coordination number in FeCe-SAD/HPNC was about 4, while the coordination number of Fe-Ce bond was about 1, which implies a direct bonding between Fe and Ce in the FeCe-SAD/HPNC [94]. In addition, the Ce wavelet transform in FeCe-SAD/HPNC showed Ce-N and Ce-Fe scattering peaks at 3.5 and 6.9 Å, respectively (Fig. 9(b)) [94]. The fabricated FeCe-SAD/HPNC catalysts exhibited excellent activities comparable to 20 wt% Pt/C and far superior to other catalysts in 0.1 mol/L $HClO_4$ solution and assembled into H_2-O_2 PEMFC (Figs. 9(c) and 9(d)) [94].

Interestingly, the preparation of M_1-M_2 catalysts with dual dissimilar metal sites inevitably results in the coexistence of multiple active site configurations, such as M_1-N_4, M_2-N_4, and M_1-M_2-N_x. The synergistic effects arising from the interaction between these different active sites also contribute to enhanced ORR performance. However, most studies to date have not fully characterized these overlapping active sites. Therefore, there is still much to explore in terms of the precise design and understanding of the interactions between M_1-N_4, M_2-N_4, and M_1-M_2-N_x in dual metal center catalysts.

3.3.5 Multi-metallic site catalysts

Multi-metallic site catalysts are developed by incorporating additional metals into bimetallic sites, enriching the central metal atoms in the active sites. While multi-metallic sites offer the potential to enhance the ORR activity, the effect on the electronic structure is often more complex, and the interactions between metal atoms can lead to unpredictable outcomes. One of the challenges in designing multi-metallic catalysts is achieving effective synergy between the metals, which can maximize their individual contributions and create a catalyst with superior ORR performance.

Liu et al. [95] investigated this concept by impregnating electrospun PAN nanofibers with a mixed solution of iron nitrate, cobalt nitrate, and nickel nitrate, followed by heat treatment in NH_3 to form FeCoNi-N/CNFs catalysts. They then explored the relationship between the ratio of Fe/Co/Ni in the active sites and the activity of the catalyst. XPS spectroscopy revealed that when the ratio of Fe/Co/Ni was 4:2:1, the contents of the components responsible for higher ORR were maximized. At this optimal ratio, the onset potential and peak densities for the FeCoNi-N/CNFs and Pt/C catalysts were 0.74/0.61 V and 0.73/0.60 V, respectively (Figs. 9(e) and 9(f)) [95]. This study highlights the promising enhancement of ORR activity through multi-metallic site catalysts.

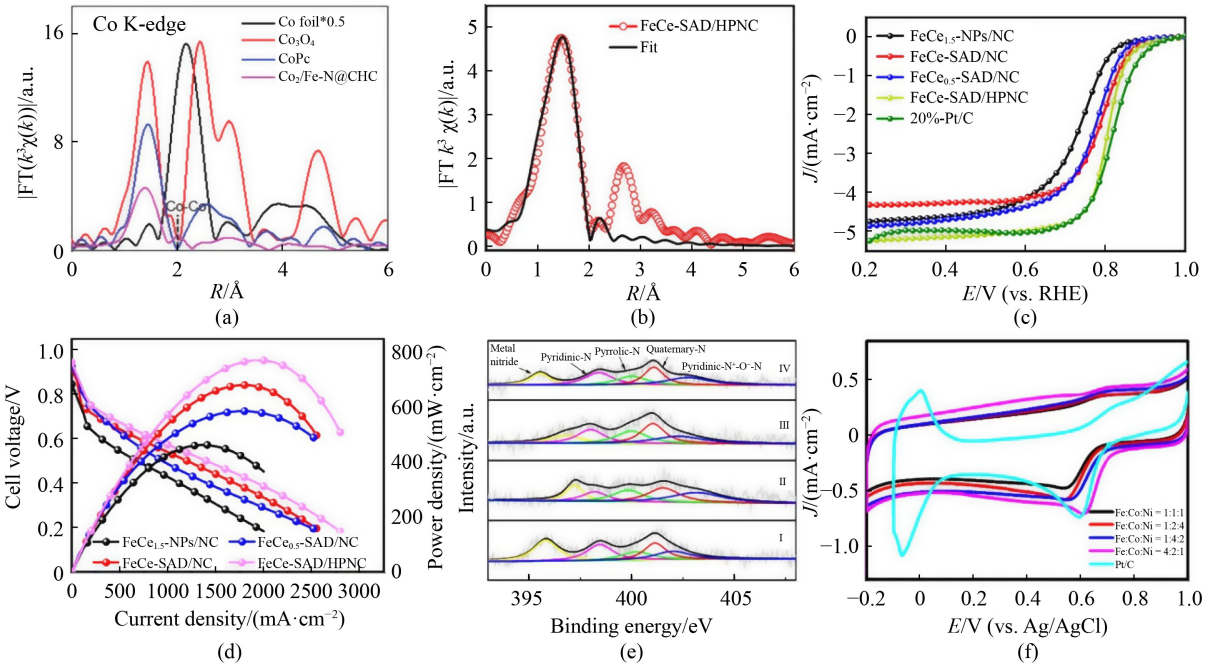

Fig. 9 Structural characterization and performance evaluation of Bi-/multi-metallic active site catalysts.

(a) Co K-edge FT-EXAFS spectra of Co_2/Fe-N@CHC, Co foil, Co_3O_4, and CoPc (adapted from Wang et al. [93] under the terms of CC BY-NC license); (b) EXAFS fitted image in R-space of FeCe-SAD/HPNC; (c) LSV curves of catalysts prepared by Fe and Ce in different ratios in 0.1 mol/L $HClO_4$ electrolyte; (d) performance image of H_2-O_2 PEMFC assembled with different catalysts (adapted with permission from Yang et al. [94], copyright 2023, American Chemical Society); (e) XPS survey of FeCoNi-N/CNF catalysts with different Fe/Co/Ni ratio: (I) 1:1:1, (II) 1:2:4, (III) 1:4:2, and (IV) 4:2:1; (f) CV curves of FeCoNi-N/CNF catalysts with different Fe/Co/Ni ratio and commercial 20%Pt/C catalyst (adapted with permission from Liu et al. [95], copyright 2018, Elsevier).

However, despite the observed improvement, there still remains significant room for further research into multi-metallic site catalysts. The overly complex interactions between different active center metals present a major challenge, and optimizing these interactions for higher ORR activity requires more in-depth exploration.

3.4 Modulating carbon materials

The macroscopic morphology and microscopic composition of the carbon material structure have an important impact on the catalytic ORR performance [96], especially the intrinsic activity of the catalyst. In recent years, various strategies have been explored to enhance the ORR activity, but there have always adverse effects. For example, increasing the graphitization degree of the carbon material can enhance their stability, but it does not always effectively enhance the intrinsic ORR activity. Therefore, it is critical to actively modulate the carbon material to optimize its interaction with the active sites, thereby promoting the ORR reaction [22].

Active sites to work together to promote ORR reactions is crucial [97]. The modulation of carbon materials in terms of curvature effects and the introduction of edge carbon defects is an important strategy to modulate carbon materials in recent years.

3.4.1 Curvature effects

Curvature refers to the degree of curvature of a curve or surface at a given point; the greater the curvature, the more pronounced the bend in the curve or surface. In the case of carbon nanotubes, curvature is defined as the reciprocal of the inner radius. The curvature of carbon materials plays a pivotal role in modifying their nanostructures, which not only promotes mass transfer but also enhances activity and stability by lowering the d-band center energies of the metal atoms at the center of the active sites, thereby inhibiting the adsorption of oxygen-containing species and better controlling the interactions between the active sites and reactants.

For example, Chen et al. recently reported the preparation of a dense distribution of FeN_4 sites on layered porous carbon with a highly curved surface, creating the FeN_4-hcC catalyst with FeN_4 sites. This catalyst was synthesized by pyrolyzing the surfactant poly (ethylene oxide)-poly (propylene oxide)-poly (ethylene oxide) (PEO_{20}-PPO_{20}-PEO_{20}(P123)) modified Fe-zeolitic imidazolate framework (ZIF)-8 precursor (P123@Fe-ZIF-8), forming an onion-like carbon structure. The d-band center of FeN_4-0.023 (0.023 is the curvature $c = 1/R$, where R refers to the radius of the sphere) was found to be lower than that of FeN_4-0 catalyst (Table 2) [98]. This downward shift in the

Table 2 Changes in the electronic structure of Fe-N_4 sites and coordination environment at different curvatures

Model	Fe-N bond length/Å	Bader charge	d-band center (UP)/eV	$\Delta G_{deformation}$/eV
FeN_4-0	1.892	1.145	–1.831	–1.35
FeN_4-0.012	1.900	1.179	–1.857	–1.21
FeN_4-0.017	1.906	1.174	–1.865	–1.20
FeN_4-0.023	1.914	1.166	–1.871	–1.18

d-band center weakens the adsorption of oxygen-containing intermediates, such as *OH, making it easier for them to desorb. Furthermore, the Gibbs free energy for *OH desorption was calculated to be higher for FeN_4-0.023 compared to that for FeN_4-0 (the d-band centers of FeN_4-0.023 and FeN_4-0 have ΔG_{*OH} of 0.68 and 0.60 eV, respectively). This suggests that *OH is more readily desorbed on FeN_4-0.023, while at the same time both catalysts use *OH desorption as the RDS for ORR (Fig. 10(a)) [98], which proves that ORR kinetics are faster on FeN_4-0.023 catalysts.

In another study, Li et al. synthesized a single-atom Fe-NC catalyst Fe-N_4 sites uniformly distributed on the surface of mesoporous metal organic framework (MOF)-derived carbon nanorods. The curvature of the carbon substrate was regulated through the self-assembly of the mesoporous MOF. DFT theoretical calculations showed that the curvature modulates the charge density around FeN_4, which affects the adsorption strength of the intermediate on the active site and further promotes the ORR rate. The $E_{1/2}$ of the L/Fe-NC (large mesoporous catalyst) was found to be 0.82 V in 0.5 mol/L H_2SO_4 (Fig. 10(b)) [99]. The theoretical calculations revealed that the low-curvature Fe-NC catalysts had a lower charge density than that of high curvature (hc-Fe-NC) or convex surface (v-Fe-NC) activities, further supporting the importance of curvature in enhancing catalytic performance.

3.4.2 Edge defect engineering

In recent years, significant efforts have been dedicated to constructing edge-loaded M-N-C catalysts, not only because they feature tunable microporous structures and the edge-loaded active sites, but also because they provide high intrinsic activity and efficiently expose active sites. Furthermore, edge-loaded active sites can prevent atomic agglomeration due to the high metal loading. However, due to their difficult preparation, the preparation of these edge-loaded active site M-N-C catalysts still remains challenging, and simpler and more efficient synthesis strategies are still under development [100].

For example, Jiang and colleagues recently introduced I_2 during the pyrolysis process to etch the carbon matrix, along with ZnFeMM (a ZnFe nano-oxide mixed material), serving both as the iron source and etching agent. This approach effectively etched the carbon matrix into edge carbons and doped them with FeN_4, successfully synthesizing an Fe-N-C catalyst enriched with edge-loaded Fe-N_4 sites, designated as e-Fe-N/CNS. Analysis of the EXAFS fitting results for the reflection paths of in-plane Fe-N, edge Fe-N, and Fe-C bonds, in comparison to the edge FeN_4 configuration simulated by DFT calculations in the R-space revealed that edge Fe-N is the dominant active-site configuration in e-Fe-N/CNS (Fig. 11(a)) [101].

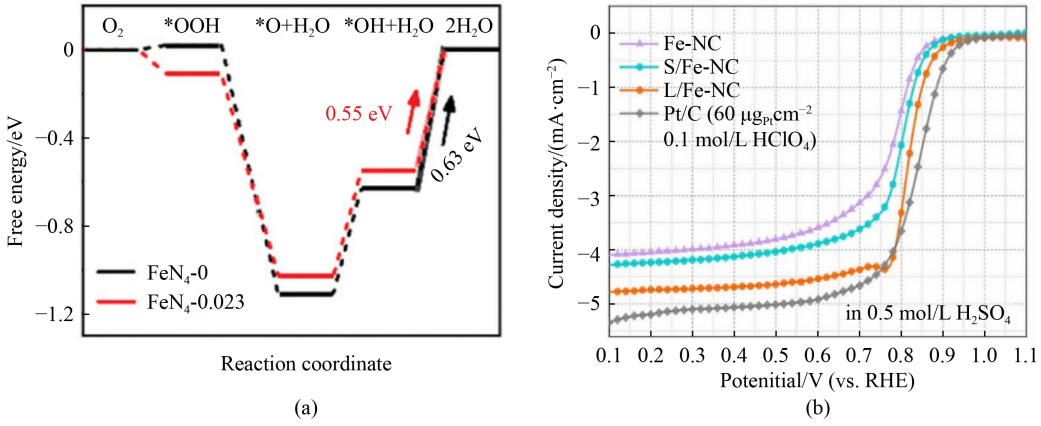

Fig. 10 Impact of curvature effects on adsorption energetics and catalytic performance.
(a) Gibbs free energy curves for ORR at equilibrium potential (U = 1.23 V) for FeN_4-0 and FeN_4-0.023 models (the arrows indicating the RDS) (adapted from Chen et al. [98] under the terms of CC BY license); (b) ORR polarization curves of L/Fe-NC, S/Fe-NC, and Fe-NC in 0.5 mol/L H_2SO_4 (adapted with permission from Li et al. [99], copyright 2023, Elsevier).

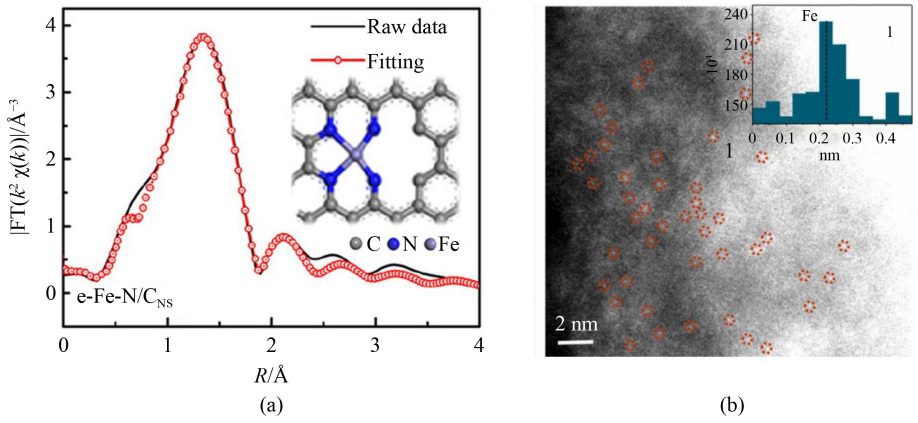

Fig. 11 Structural characterization of edge-defect sites.

(a) Comparison of the experimental FT-EXAFS spectra of e-Fe-N/CNS and the fitted curves of the simulated edge Fe-N_4 configurations (adapted with permission from Jiang et al. [101], copyright 2023, American Chemical Society); (b) AC-HAADF-STEM images of FeSA-N/Cs-OAc, X-Y inset shows strength profiles (adapted with permission from Kong et al. [102], copyright 2022, Elsevier).

In addition, AC-HAADF-STEM images of cavity-edge FeN_4 active sites showed highly dispersed bright spots at the pore edges, clearly representing Fe atoms located at the edge-bearing Fe-N_4 sites, (Fig. 11(b)) [102]. The $E_{1/2}$ of the FeSA-N/Cs-OAs catalyst prepared concurrently was found to be 0.82 V in 0.1 mol/L $HClO_4$ solution, with a maximum output power of 640 mW/cm^2 in an H_2-O_2 fuel cell.

In another approach, Cui et al. achieved a maximum output power of 640 mW/cm^2 by combining hydroxyl functionalization with NH_4Cl-assisted etching using CuN_4 as the active site (CuSAs@DCSs). The introduced NH_4Cl etching promoted the preferential formation of edge-bearing CuN_4 while enhancing carbon edge formation. The prepared catalysts exhibited impressive ORR performance [103].

In addition, a recent study proposed a molecularly engineered anchored carbon platform (ACP)-based synthesis method to stabilize M-N (M = Fe, Co, Ni, Cu) edge-active sites on carbon carriers. This molecularly engineered ACP-based catalyst exhibited superior stability compared to commercial Pt/C in an ORR reaction across a wide pH range. This ACP-based scheme not only advances the preparation of edge-hosted active sites catalysts but also opens the possibility for using diverse central metal atoms, thus expanding the potential for creating highly active and stable ORR catalysts [104].

Recent studies have employed various strategies to prepare catalysts aimed at enhancing the intrinsic activity of active sites (Table 3). However, catalysts developed using a single strategy often fail to optimize both activity and stability. To address this limitation, researchers must combine multiple strategies, based on existing methods, to effectively balance and enhance both activity and stability, thereby overcoming the trade-off between the two.

4 Enhancing active site density

It is well known that single-atom catalysts have higher specific surface areas than nanoparticle catalysts or bulk catalysts, leading to enhanced activity in ORRs. However, it is difficult to prepare highly dispersed and

Table 3 Catalysts prepared with different strategies for enhancing intrinsic activity

Strategies	Catalysts	$E_{1/2}$	Stability	Fuel cell performance
Tuning the coordination structure of the central atom	CoN_3O SAC	0.849 V (0.1 mol/L $HClO_4$)	10 mV (30000 cycles)	978 mW/cm^2 (2 bar H_2/O_2) [105]
	Mn-pr-N-CG	0.896 V (0.1 mol/L $HClO_4$)	2 mV (10000 cycles)	/[106]
Heteroatom doping	Mn-N-C-S	0.80 V (0.1 mol/L $HClO_4$)	4 mV (10000 cycles)	820 mW/cm^2 (2 bar H_2/O_2) [107]
	FeNCP	0.80 V (0.5 mol/L H_2SO_4)	35 mV (10000 cycles)	880 mW/cm^2 (2 bar H_2/O_2) [72]
	Fe-N-C-P/N, P-C	0.80 V (0.1 mol/L $HClO_4$)	2 mV (5000 cycles)	625 mW/cm^2 (2 bar H_2/O_2) [74]
	Fe/Co-N-C-x	0.81 V (0.5 mol/L H_2SO_4)	13 mV (10000 cycles)	466 mW/cm^2 (2 bar H_2/O_2) [108]
Dual/multi-metal sites	$Fe_{SA}Cu_{SA}$/NC	0.86 V (0.1 mol/L $HClO_4$)	0 mV (10000 cycles)	912 mW/cm^2 (2 bar H_2/O_2) [109]
	Fe_2-$S_1N_5N_5$/SNC	0.829 V (0.1 mol/L $HClO_4$)	26 mV (5000 cycles)	810 mW/cm^2 (2 bar H_2/O_2) [110]
Modulating carbon materials	Fe_{SA}-N/TC	0.825 V (0.1 mol/L $HClO_4$)	5 mV (5000 cycles)	1100 mW/cm^2 (2 bar H_2/O_2) [111]
	FeN_4-SMX	0.83 V (0.1 mol/L $HClO_4$)	16 mV (60000 cycles)	1086 mW/cm^2 (2 bar H_2/O_2) [112]

structurally well-defined single-atom catalysts, not only due to the migration and aggregation of metal atoms during high-temperature treatments because of the higher free energy gained, but also due to the weak interactions between metal atoms and the carbon matrix/nitrogen. These weak interactions prevent the metal atoms from following the established structure, which leads to deviations from the desired single-atom configuration [113,114]. Instead of focusing solely on increasing metal loading through higher precursors concentrations, it has been possible for some time to increase the density of active sites actually involved in the ORR by continuously improving synthesis methods [115], by altering the electronic structure to enhance the interactions between the metal-loaded active sites and the carbon matrix/nitrogen, or by designing structures that can expose a larger number of active sites for the reaction [116,117].

4.1 Strengthening the M-N bond

In the active site of the M-N_4 configuration, the metal ion is coordinated with the nitrogen ligand, and the entire active site is connected to the carbon matrix. However, during high-temperature treatment, the metal ions tend to agglomerate because the M-M bond is more stable than the M-N bond. Therefore, enhancing the interaction between metal ions and the surrounding ligands has become a difficult issue. To address this, several strategies have been developed to enhance the connection between the metal ions and the ligands [116], to increase the density of active sites. These strategies include chelation, adsorption, and defect engineering [117].

4.1.1 Chelation strategies

Some non-metallic elements, such as N, O, P, and S, have lone pair electrons. When these elements coordinate with metal ions via lone pair electrons, they act as “claws” to hold the metal ions firmly in place, forming extremely stable coordination configurations. This helps prevent the metal ions from agglomerating during high-temperature treatments. Wang et al. reported a chelation strategy for synthesizing Fe-N-C catalysts using PDANFe(III) complexes as precursors. In this approach, the *in situ*-grown FeN_x active sites were uniformly deposited on the carbon surface (Fig. 12(a)) [118], and the catalysts obtained had high ORR activity due to more accessible active sites and high porosity.

In a similar study, Zhang and his coworkers proposed an iron-coordinated self-assembly method to prepare iron-chelated pyridine nitrogen-rich coordination nanosheets (IPNCN) composites as electrocatalysts. The coordination unit in IPNCN is a tetrapyridylphenazine, which has a rigid planar structure with complete conjugation. Since both ends of the coordination unit are pyridine nitrogen atoms that chelate with Fe, the Fe and the four pyridine nitrogens form an Fe-N_4 coordination structure. The prepared IPNCN composites exhibited excellent electrocatalytic activity, with an E_{onset} of 0.93 V, an $E_{1/2}$ of 0.84 V, and a higher resistance to methanol toxicity and electrochemical durability (Fig. 12(b)) [119]. In a previous study, it was demonstrated that pyridinic nitrogen and graphitic nitrogen greatly promoted the ORR activity in the IPNCN, with pyridinic nitrogen uniformly and stably dispersed (Fig. 12(c)) [119].

Despite the C-N bond breakage at higher pyrolysis temperatures, the pyridine nitrogen content in IPNCN still enables the catalyst to maintain high activity. In addition to Fe-N-C catalysts, other catalysts have also garnered attention for their effective ORR performance. Xu et al. successfully synthesized a Mn-N_x site catalyst that was tightly linked together by the chelating effect of chitosan and manganese ions through the dispersion of Mn atoms in a chitosan hydrogel-derived carbon matrix [120]. Chitosan is used as a precursor due to its abundant free amino groups, and these free amino groups and free hydroxyl groups can act as a “claw” to capture Mn^{2+} ions and prevent Mn^{2+} from uncontrollable agglomeration and migration during the subsequent pyrolysis process. After pyrolysis, this structure connected by chelation was transformed into an active site coordination structure of Mn-N_x and firmly anchored to the carbon matrix. The resulting Mn-N-C catalyst exhibited excellent ORR activity, with an $E_{1/2}$ of 0.86 V and excellent stability, retaining 93% of its initial current value after 10 h.

In another study, Xia and coworkers developed a method of intertwining the prepared amine group quantum dots into the carbon matrix to provide numerous anchoring sites, which stabilizes and homogeneously disperses the quantum dots on the surface of the carbon substrate and restricts metal aggregation through the chelation between the metal cations and amine groups. During freeze-drying, this strong chelation leads to the interconnection of the quantum dots and their self-assembly into a layered block-like structures [121]. Notably, some nitrogen-containing species, oxygen-containing functional groups, SCN^-, and phytanic acid, and other ligands, which can form strong interactions with the metal ions, are frequently utilized as ligand sites for anchoring metals, further enhancing the stability and performance of metal-ion-based catalysts.

4.1.2 Defect capture strategy

In non-PGM single-atom catalysts, defects in the carbon matrix play a crucial role in tuning the coordination structure of the central metal atom [122,25]. Additionally, these defects serve as an effective strategy to anchor the active site to the carbon matrix [123,124]. Recently, Yao et al.

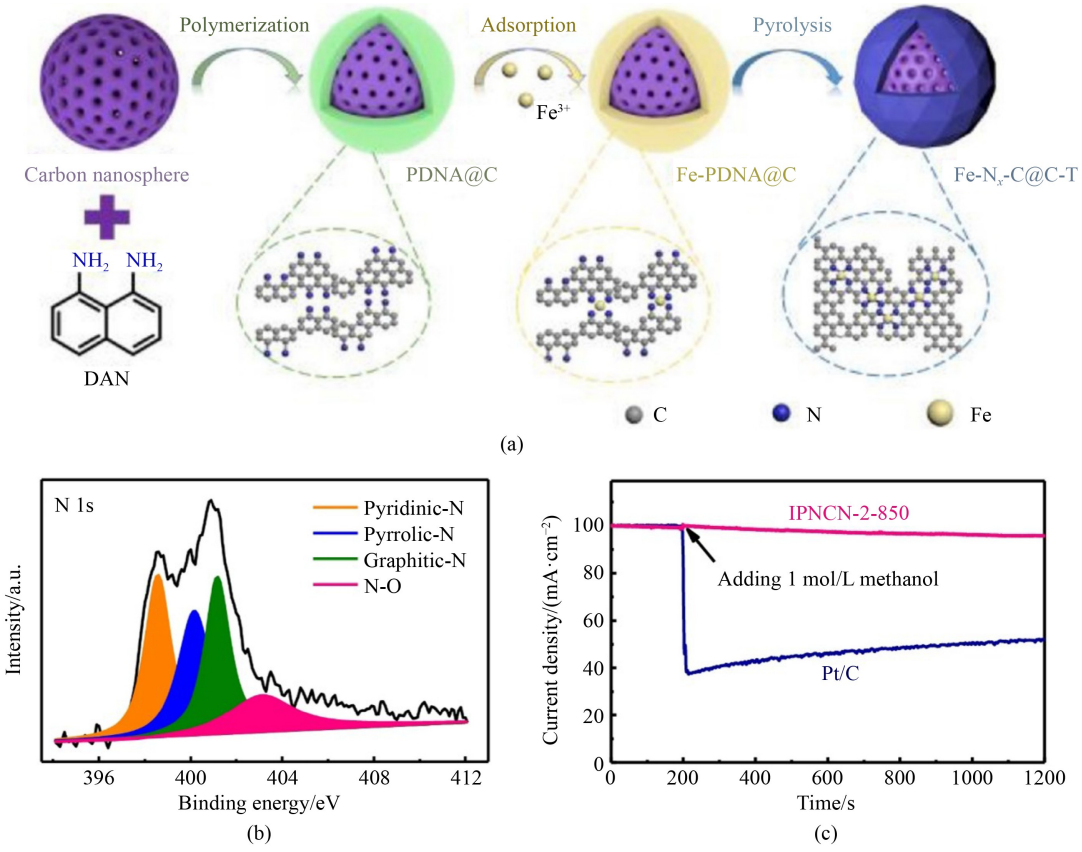

Fig. 12 Chelation-engineered catalyst synthesis: structural optimization and performance enhancement.
(a) Schematic synthesis of Fe-N_x-C@C-T catalysts (adapted with permission from Wang et al. [118], copyright 2023, Elsevier); (b) the high-resolution N 1s, XPS spectra of the IPNCN-2–850 composites; (c) methanol tolerance evaluation of the IPNCN-2–850 composite and Pt/C catalysts (adapted from Zhang et al. [119] under the terms of CC BY license).

prepared a single-atom copper catalysts (CuSACs) with abundant carbon defects using a salt-assisted pyrolysis strategy. The density of these defects in the catalyst was modulated by adjusting the content of $ZnCl_2$, which acts as a pore generator. Since $ZnCl_2$ can be used as an etcher to produce mesopores, specifically, during pyrolysis, the pore size increased with the content of $ZnCl_2$ decreasing, while the total pore volume and specific surface area gradually increase (Fig. 13(a)) [125]. However, when the $ZnCl_2$ content reached a certain value, the pore structure and specific surface area began to decrease. In addition, the use of KOH as a strong etchant can result in an ultrahigh specific surface area for CuSACs, mainly due to the creation of micropores (Table 4) [125].

DFT calculations demonstrated that the carbon defects in CuSACs after $ZnCl_2$ salt-assisted pyrolysis can significantly reduce the charge density of the O-O bonds in the intermediate OOH*, resulting in a lower dissociation energy and thus a more excellent ORR activity. Similarly, Yang et al. used a solid-phase thermal diffusion strategy to prepare an isolated single-atom site catalyst (ISASC). Under high temperature conditions, the Mn element was detached from the core-MnO_2 lattice, captured by carbon defects generated during shell-ZIF-8 carbonization, and reduced to Mn atoms. These nitrogen-coordinated manganese sites were subsequently converted into a tetra-nitrogen-coordinated manganese (Mn $SAsN_4$) site catalyst by treatment with NH_3. The resulting catalysts showed excellent ORR activity and durability in 0.1 mol/L $HClO_4$ [126].

When defect engineering and heteroatom doping synergistically modulate the electronic structure of the coordination environment around the active site, the resulting changes can lead to higher activity of the prepared catalysts. Zhao et al. reported an N and S co-doped single-atom catalyst with Fe-N_3S_1 as the active site and abundant vacancy defects. This catalyst benefited from the “vacancy defect sensing effect” and the “vacancy defect inducing effect” (Fig. 13(b)) [127]. The catalyst exhibits high catalytic activity, selectivity, and stability in 0.5 mol/L H_2SO_4. DFT calculations showed that S affects the catalyst synergistically by causing an upward shift of the d-band center of the metal atoms, which promotes O_2 adsorption. Additionally, the vacancy defects around the active site helped balance the formation of OOH* and the reduction of *OH, further improving the ORR performance.

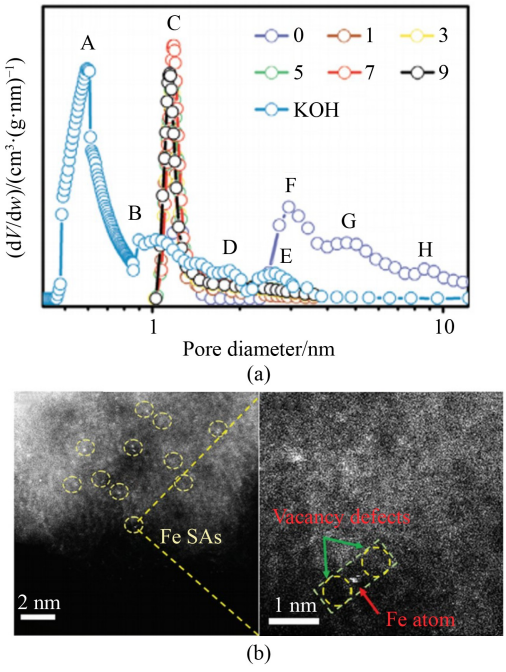

Fig. 13 Structural modulation of catalysts through engineered defects.

(a) Pore size distribution of the Cu-SACs synthesized under different conditions (adapted with permission from Yao et al. [125], copyright 2023, John Wiley and Sons); (b) enlarged AC-HAADF-STEM image of Fe SAs/NSC-vd and Fe SAs/NSC (adapted with permission from Zhao et al. [127], copyright 2023, John Wiley and Sons).

Table 4 Relationship between precursor mass and pore structure of Cu-SAC-X catalysts

Catalysts	BET surface area/ ($m^2 \cdot g^{-1}$)	Adsorption total pore volume/ ($cm^3 \cdot g^{-1}$)	Adsorption average pore width/nm
Cu-SACs-0	60.55	0.12	8.04
Cu-SACs-1	916.55	0.57	1.62
Cu-SACs-3	1537.88	0.96	1.33
Cu-SACs-5	1521.2	0.83	1.28
Cu-SACs-7	1597.99	1.08	1.33
Cu-SACs-9	1440.24	0.86	1.27

4.1.3 Cascade anchoring strategy

Compared to the catalysts prepared by the previously mentioned strategies, the catalysts prepared by using the cascade anchoring strategy possessed higher metal loading. For example, while chelation and defect engineering strategies have been developed, metal loading always undergoes unavoidable agglomeration and migration during high-temperature treatments, which reduces the density of the active sites (generally not exceeding 4 wt%, which prevents the catalysts prepared by these methods from being commercialized on a large scale [128]. Zhao et al. introduced a cascade anchoring strategy which allowed the preparation of various M-NC SACs (M = Mn, Fe, Co, Ni, Cu, Mo, etc.) with metal loadings up to 12.1 wt%. In this strategy, metal ions were first anchored to the carbon matrix using a chelating agent such as glucose (first-level anchoring). An excess amount of chelating agent was then added to the carbon matrix as a physical isolation layer to further hinder the metal ions from agglomerating (secondary anchoring). This mixture is then combined with melamine and heated at high temperature, during which the residual material on the carbon matrix will decompose at about 500 °C as a physical isolation layer to protect the metal atoms (tertiary anchoring). Finally, at temperatures higher than 500 °C, melamine decomposes and forms the M-N_x coordination structure, which is anchored to the carbon substrate (tertiary anchoring) (Fig. 14(a)) [129]. Catalysts prepared using this sequential anchoring method have a higher density of active sites and, naturally a higher metal loading. Since chelation can occur between a wide range of metal ions and ligands, the cascade anchoring strategy is a versatile and commercially available strategy for preparing non-PGM single-atom catalysts with very high ORR activity. In a recent study, Du and colleagues applied a cascade anchoring strategy to anchor atomically dispersed FeN_5 sites onto porous biochar (Fe-N-FPBC), which achieved high loading through tertiary anchoring of the FeN_5 sites on the support platform [130]. In fact, the measures of anchoring or protecting the metal species in advance, followed by the presence of further protection during subsequent preparation are all part of the cascade anchoring strategy. Moreover, Hai et al. recently reported a synthesis method for ultra-high-density (UHD) single-atom catalysts with metal loadings up to 23 wt%, combining impregnation and two-step annealing (Fig. 14(b)) [131]. The first step of annealing saturates the metal surface by selectively removing the metal ligands, allowing for high coverage metal anchoring on the support surface. In the second step, cleaning removes unbound species and completely removes ligands, thus ensuring high metal loading. This two-step annealing method, based on the cascade anchoring method, is also a general method for preparing highly metal-loaded single-atom catalysts.

4.2 Spatial confinement

The spatial confinement effect, as the name suggests, restricts the aggregation and migration of metal atoms by using a space comparable to the scale of metal atoms, which in turn increases the number and density of active sites. Such confined spaces can be obtained by using MOFs or COF materials as precursors [30,132,133], which can be attributed to the fact that MOFs materials possess high porosity, and their high porosity can be used as a space for immobilizing metal atoms to reduce the degree of unavoidable aggregation and migration during

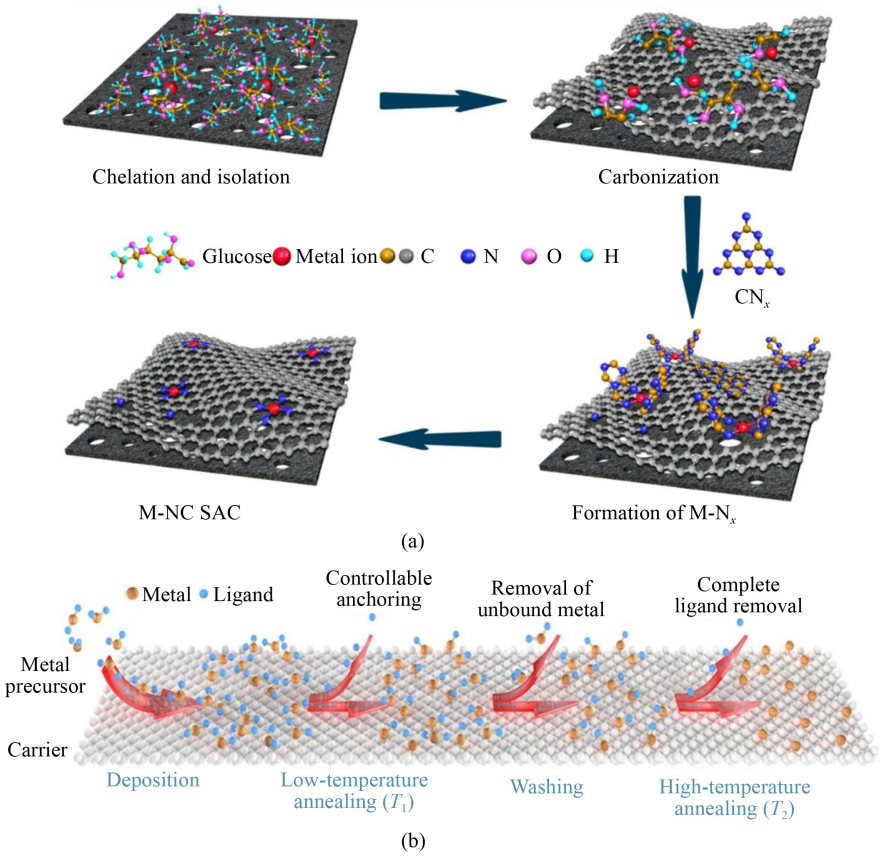

Fig. 14 Schematic illustration of the cascade anchoring strategy.

(a) Schematic representation of a generic method for the synthesis of M-NC SAC with metal loading of 12.1 wt% (adapted from Zhao et al. [129] under the terms of CC BY license); (b) strategy for the preparation of UHD-SACs (adapted with permission from Hai et al. [131], copyright 2021, Springer Nature).

high-temperature pyrolysis [134,135].

ZIF-8 is often used as a precursor for the preparation of electrocatalysts due to its unique structure, where $Fe(acac)_3$ is encapsulated inside the ZIF-8 framework to create cavities, which is attributed to the fact that the diameter of ZIF-8's cavity is 11.8 Å larger than 9.7 Å of $Fe(acac)_3$. During pyrolysis, the $Fe(acac)_3$ molecule is bounded within a ZIF-8 cavity, which eventually forms a single-atom catalyst (Fig. 15(a)) [136]. In addition, covalent organic framework (COF), as a porous crystalline material, can also be utilized to create highly dispersed active sites from its pores. Yang et al. encapsulated the ZIFs in the pore channels of the COFs by in situ growth, and then converted the ZIFs into active sites during subsequent pyrolysis. The catalysts prepared in this way possessed very high ORR activity, which is attributed to the presence of ZIFs located in the COF pore channel structure the active sites are greatly restricted in spatial migration and aggregation (Fig. 15(b)) [137].

In addition to achieving spatial confinement through the formation of cages by the unique structure of the MOF or COF, it is also possible to confine the metal species in the active sites by species such as, for example, Si. Previous studies have shown that covering the surface of the carbon matrix with a layer of SiO_2 during the synthesis of single-atom catalysts can inhibit the occurrence of aggregation of Fe by lowering its surface energy and thereby inhibiting it, due to the ability of SiO_2 to promote the formation of M-N_x species [138], which increases the interactions between metal atoms and nitrogen atoms, and additionally traps volatiles during pyrolysis to produce a porous structure. The catalysts prepared by this method possess high ORR activity. Deng and colleagues prepared an Fe-SAC with up to 80% utilization efficiency (UE) using a strategy of confined pyrolysis with SiO_2, by covering the polydopamine nanospheres with a layer of SiO_2, introducing a mixture of precursors for pyrolysis, and then completely removing the excess metal species and SiO_2 shells from the surface via etching, followed by secondary pyrolysis, so that the Fe atoms reach the surface under the carbon nanospheres by diffusion instead of all entering into the interior of the carbon matrix, which further increases the accessibility of the active sites. In addition, the SiO_2 layer was removed during pyrolysis, and the Fe-SACs prepared by this method do not need to have high Fe loading to obtain high ORR activity due to the high exposure rate of the active sites (Fig. 15(c)) [139]. Gu et al. similarly also

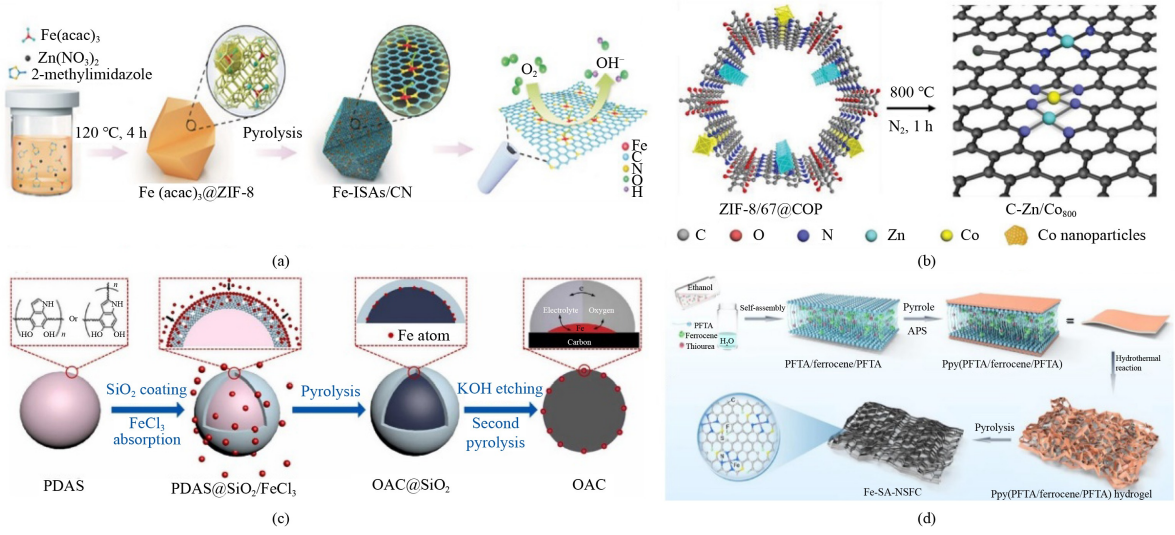

Fig. 15 Schematic representation of spatial confinement strategy.

(a) Schematic synthesis of Fe-ISAs/CN catalysts (adapted with permission from Chen et al. [136], copyright 2017, John Wiley and Sons); (b) schematic diagram of the synthesis process of C-Zn/Co 800 catalysts (adapted with permission from Yang et al. [137], copyright 2023, John Wiley and Sons); (c) schematic of CNS preparation with dispersion of Fe atoms at the three-phase boundary (adapted with permission from Deng et al. [139], copyright 2022, Elsevier); (d) schematic synthesis of Fe-SA-NSFC (adapted from Zhou et al. [142] under the terms of CC BY license).

reported a method to fabricate Cu monolithic atoms by utilizing the confined space between a template and a SiO_2 wall in SBA-15 (TOS). In this preparation method, the inherent confined space and abundant Si-OH groups in TOS are extremely important for the anchoring of Cu atoms. Since it does not require the metal atoms to possess unique properties, this preparation method is versatile and can be applied to other metals like Co, Ni and Zn as well [140]. Furthermore, a recent study reported a cobalt-based activated carbon cathode catalyst (Co-CNF) prepared by combining a SiO_2-limited pyrolysis strategy and utilizing the unique structure of ZIF, which avoids destroying the unique structural morphology of ZIF during direct pyrolysis of ZIF. The catalysts synthesized using this method have higher ORR activity [141]. Although SiO_2 plays an indispensable role in the preparation process, a subsequent acid treatment is still required to remove the excess SiO_2, which is unfriendly to the catalysts and very prone to reduce the metal loading. Zhou et al. developed an innovative strategy where metal precursor was embedded in a multilayer film of perfluorotetradecanoic acid (PFTA) and coated with a layer of polypyrrole before pyrolysis, which ultimately led to the creation of the stable multilayer construction of PFTA/ferrocene/PFTA with hydrophilic layer surface and hydrophobic layer interlayer (Fig. 15(d)) [142]. Due to the high hydrophobicity of ferrocene itself, the ferrocene was tightly confined in the interlayer. The catalysts prepared using this multifunctional multilayer stabilization method had a metal loading as high as nearly 16 wt%, which opens up a new path for enhancing the density of the active sites through spatial confinement.

4.3 Porous structure optimization

In general, ORR is kinetically slow, making it important to maximize the contact between O_2 and the active sites of catalysts. Many catalyst preparation strategies today focus only on increasing the overall density of active sites, ignoring the fact that many active sites are inaccessible to reactants such as O_2 [143], either because the active sites are buried deep inside the carbon matrix or because the pore sizes are too smaller for O_2 to reach them [144,145]. To address this, one of the key strategies for improving catalyst efficiency is the creation of well-defined three-dimensional (3D) porous structures, which not only provide sufficient three-phase boundaries for ORR to occur [146,147], but also enhance mass transfer and expose more active sites, which significantly improves the effectiveness of the catalyst [148,149].

One of the most effective strategies used in recent years to prepare porous structures is the template strategy, which includes hard template methods (e.g., using SiO_2), soft template methods that functionalizes the surface of the carbon matrix [150,151], self-sacrificial template methods, and combined multiple templates [152,153].

Although the hard template method is well-established, it often requires subsequent etching, usually with strong acids or bases, which can damage the active sites. Daniela et al. synthesized catalysts with simultaneous dispersion of Fe, Co, and N on a carbon substrate by using SBA-15 as a hard template, along with transition metal complexes with phenylalanine (Phe) ligands as

precursors. This approach resulted in catalysts with high ordered porosity and a high specific surface area. However, etching with NaOH to etch the SiO_2 template at the end of the preparation process can be detrimental to the metal species, potentially affecting the durability of the catalyst [154]. On the other hand, Lu et al. employed a Zn-assisted MgO as a hard template for the preparation of atomically dispersed Fe-N_4-site catalyst (Fig. 16(a)) [155]. MgO as a hard template only requires weak acid for treatment, compared to SiO_2, and the mesopores and macropores left after treatment are very favorable for mass transfer. Additionally, the Zn species can also evaporate during the pyrolysis, increasing porosity and enhancing the accessibility of the active sites. The Fe-N-C catalysts prepared in this way reached an $E_{1/2}$ of 0.895 V. Although the subsequent treatment of the MgO hard template method does not require strong acid for subsequent treatment, weak acid treatment is still unfavorable for metal species.

Sun and colleagues reported a mechanochemical method using NaCl as an unaltered hard template, combined with ball milling (Fig. 16(b)) [156]. No characteristic peaks of NaCl were detected during subsequent characterization, which proves that it maintains its original chemical stability, which is comparable to the traditional SiO_2 templates and does not require a subsequent chemical treatment process, but only requires repeated washing with deionized water. The catalysts produced in this way have higher porosity and stability through the NaCl templates [157].

The soft template method is another effective strategy for the construction of well-defined hierarchical porous carbon structures, which differs from the hard template method most fundamentally by the presence or absence of "self-assembly," which specifically requires the presence or absence of strong interactions between the structure-directing agent and the carbon source precursor. Catalysts synthesized using a soft template strategy with cationic surfactants such as dodecyltrimethylammonium bromide (DTAB), tetradecyltrimethylammonium bromide (TTAB), and hexadecyltrimethylammonium bromide (CTAB), specifically in the nucleation of ZIF-8 into which iron ions and surfactants can be homogeneously doped to form Fe-ZIF-8. After high-temperature treatment, iron species are directly converted into Fe-N_x species encapsulated by a carbon matrix decomposed by the surfactant. The final prepared catalyst was named Fe-N/C@surfactant. The BET results showed that the SBET of the surfactant-containing catalysts (Fe-N/C@DTAB = 751 mg/m^2, Fe-N/C@ TTAB = 641 mg/m^2, Fe-

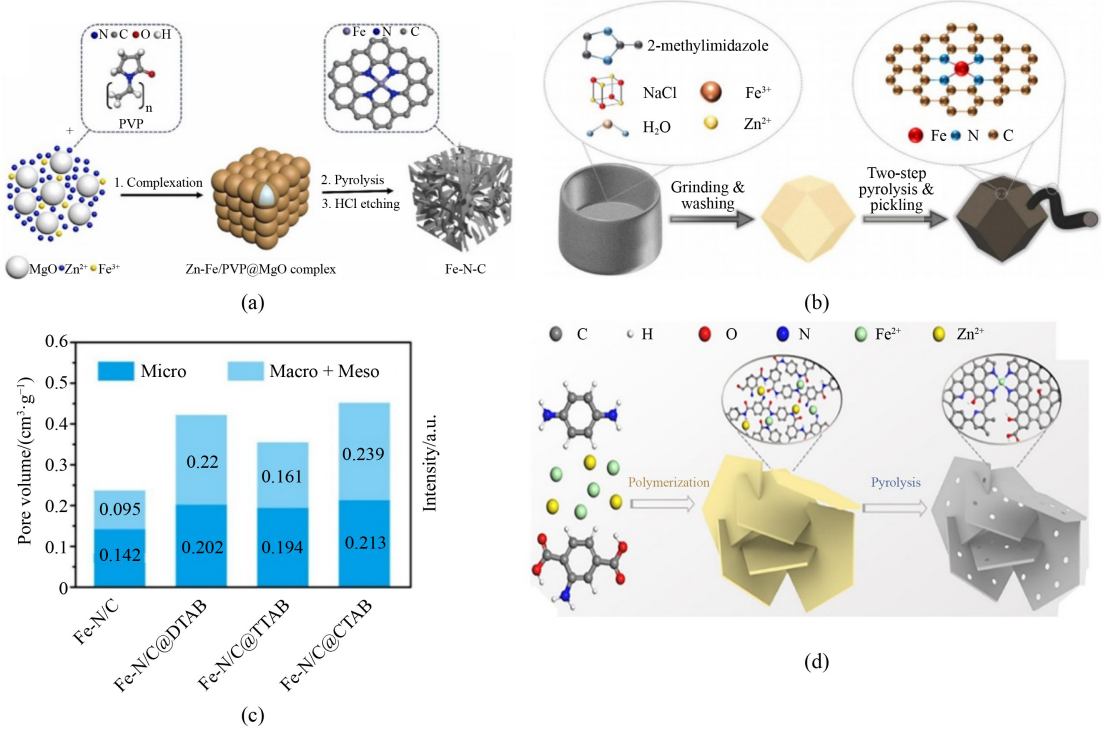

Fig. 16 Schematic illustration of porous structure with corresponding porosity distribution.

(a) Schematic synthesis of Fe-N-C catalysts prepared from Zn-assisted magnesium oxide (adapted with permission from Lu et al. [155], copyright 2022, Elsevier); (b) schematic illustration of the synthesis process (adapted with permission from Sun et al. [156], copyright 2023, Royal Society of Chemistry); (c) comparison of pore volume of catalysts with different surfactant additions (adapted with permission from Niu et al. [158], copyright 2023, Elsevier); (d) schematic synthesis of Fe-N-C SAC-T catalysts (adapted with permission from Zheng et al. [159], copyright 2024, Elsevier).

N/C@CTAB = 746 mg/m^2) was higher than that of the catalyst without surfactant (Fe-N/C = 435 mg/m^2). In addition, the pore size curves showed that the porosity of the catalysts with surfactant was also higher than that of the catalysts without surfactant (Fig. 16(c)) [158]. This was ascribed to the fact that the soft template strategy could promote the hierarchical porous structure formation, which enhanced the porosity and accessibility of the active sites.

Zheng et al. explored hydrogen-bonded organic frameworks (HOFs) as soft template for creating porous crystalline materials. These HOFs have a large specific surface area and contain abundant functional groups that can effectively anchor the metal atom sites. HOFs started to decompose above 300 °C until they were exhausted, and the Fe-N-C SAC-950 catalysts prepared using this method exhibited had an $E_{1/2}$ of 0.895 V. The pore size curves showed that the catalysts with surfactants had higher porosities than those without surfactants (Fig. 16(d)) [159].

In addition to the hard and soft templates, the self-sacrificial template strategy has also been developed. In this approach, the template itself is directly converted into the carbon material in the catalyst without any subsequent treatment. Ma et al. recently reported using ZIF-L nanorods as self-sacrificial templates to generate hollow carbon nanorods with open cavities, ZIF-8, via a simultaneous epitaxial growth process [160]. Specifically, the unstable ZIF-L was selectively converted to ZIF-8 from the outermost layer to the inner layer under the action of ethanol and (N, N-dimethylformamide) DMF mixture solution, generating ZIF-8@ZIF-L until all ZIF-L disappeared, and generating ZIF-8 with a unique hollow structure, which is extremely advantageous for the accessibility of the active sites compared to the dodecahedral structure of the traditional ZIF-8. The catalyst prepared based on this self-sacrificial template strategy naturally has high activity, and an $E_{1/2}$ of 0.80 V under acidic conditions. The catalysts are characterized by the high activity of the catalysts.

4.4 Secondary atom doping

The secondary atom doping strategy is a stepwise synthesis approach that effectively avoids the aggregation of metal atoms during the pyrolysis process and can increase the loading of metal atoms compared to the one-step synthesis strategy. This strategy involves two main steps: the doping process and the adsorption process. In the first step, the precursor undergoes carbonization, which transforms the carbon matrix into a three-dimensional porous material capable of adsorbing additional metal atoms and nitrogen sources. In the second step, more metal precursors are added, leading to the adsorption of these species onto the carbon matrix, further increasing the density of active sites.

Li et al. employed this strategy to prepare an atomically dispersed Mn-N_4 catalyst [161]. The Mn-doped ZIF-8 precursor was first carbonized and acid-treated, and the first step is known as the doping process. Then additional Mn sources were added, and the second step is known as the adsorption process. Since the carbonization process in the first step transforms the carbon matrix into a three-dimensional porous material capable of adsorbing additional metal atoms and nitrogen sources, thus increasing the density of active sites, the catalysts were prepared with an $E_{1/2}$ up to 0.80 V under acidic conditions and with good stability. Guo et al. also applied the secondary doping method to synthesize catalysts with a higher density of Mn-N_4/CoN_4 active sites (Fig. 17(a)) [162]. Their catalysts had higher defect concentrations without changing the morphology compared to those prepared by direct bimetallic atomic doping, resulting in excellent ORR activity in 0.1 mol/L $HClO_4$.

In addition, Qu and colleagues prepared a catalyst containing a high density of active sites (Fig. 17(b)) [163], named Fe-N-C-meso-evap, in which the addition of sulfate in the first step of the pyrolysis process induced the creation of a large number of mesoporous structures in the Fe-N/C catalysts, which is friendly to the Fe source added in the second step of pyrolysis. This process not only trapped the Fe source, but also greatly improved the stability and accessibility of the Fe-N_x active sites. The Fe-N/C catalysts exhibit good ORR activity and stability under acidic conditions.

This stepwise secondary atom doping strategy offers several advantages: it avoids one-step doping of metal species, reduces the risk of metal aggregation, and allows for better control over the active site density. Additionally, the first step of pyrolysis allows for shaping or modification of the carbon material, which enables the subsequent active sites to be controlled to a large extent.

5 Conclusions and perspectives

The performance of cathode catalysts is a critical factor in PEMFCs. Traditionally, platinum group metals have been widely used due to their excellent catalytic activity, but their high cost and limited durability hinder commercial viability. Consequently, significant attention has shifted to non-PGM single-atom catalysts, which offer the potential to achieve both high performance and stability. This review focuses on strategies aimed at enhancing the catalytic activity and increasing the active site density of M-N-C catalysts.

The ORR mechanism plays a pivotal role in determining the catalytic activity of M-N-C catalysts. High-performance M-N-C catalysts selectively promote the 4-electron ORR pathway, accelerating the reaction rate by optimizing the adsorption of intermediates such as

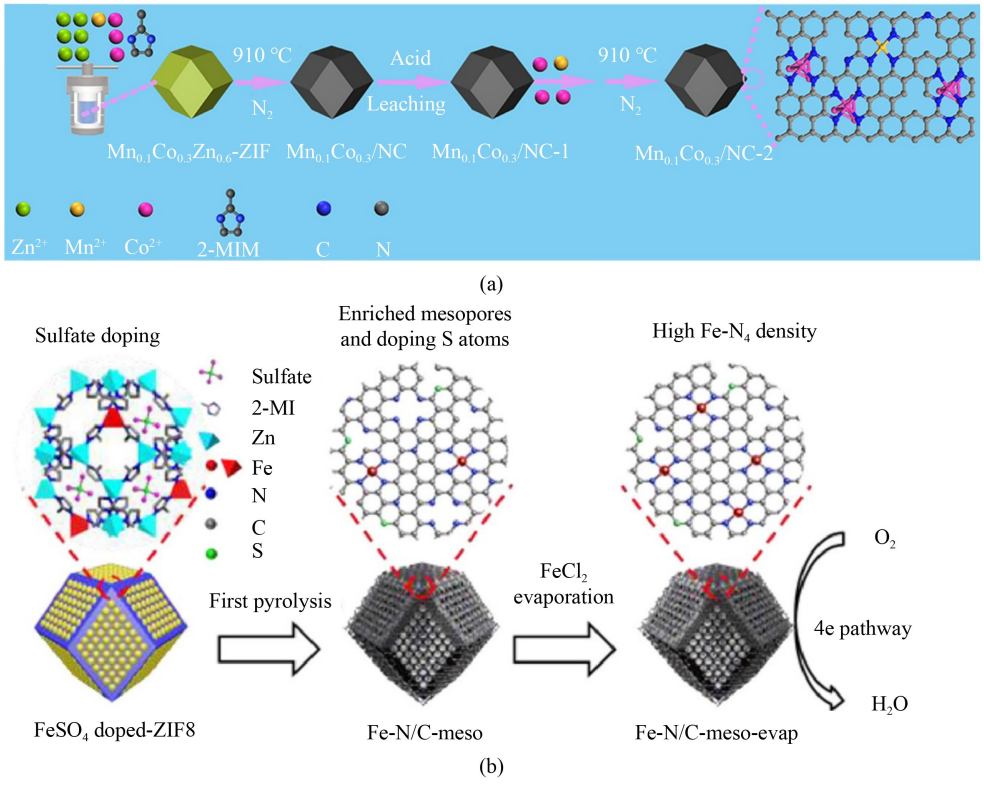

Fig. 17 Schematic illustration of secondary atomic doping strategy.

(a) Schematic diagram of the Mn/Co bimetallic synthesis route (adapted with permission from Guo et al. [162], copyright 2023, Royal Society of Chemistry); (b) schematic synthesis of Fe-N/C-meso-evap catalysts (adapted with permission from Qu et al. [163], copyright 2022, Elsevier).

OOH*. Strategies to modulate the microenvironment around active sites, including adjusting the nitrogen coordination of the central metal atom, altering M-N bond lengths, and doping heteroatoms, effectively tune the electronic structure of the active site. These modifications enhance the adsorption/desorption of intermediates, improving ORR kinetics. Additionally, constructing bi- or multi-metallic sites creates an ideal bridge adsorption model, facilitating O-O bond breaking and further boosting catalytic performance. The carbon substrate also plays a crucial role; introducing curvature or defects around active sites can enhance activity, although excessive curvature remains a challenge that requires further investigation.

Increasing the density of accessible active sites is essential for improving M-N-C catalyst performance. Key challenges include exposing encapsulated active sites and maintaining atomic dispersion while increasing metal loading. Chelation strategies, defect trapping, and cascade anchoring strengthen the bond between central metal atoms and surrounding nitrogen atoms, preventing migration and agglomeration during high-temperature synthesis. These approaches significantly enhance active site density. Spatial confinement effects, which anchor active sites to the carbon substrate through external structures, further improve stability by preventing demetallization. Combining these strategies with porous catalyst designs increases the density of accessible active sites, while edge-hosted active sites at pore edges contribute to intrinsic activity. Secondary atom doping strategies enable the formation of active sites in batches, further increasing active site density. Despite these advancements, achieving a high active site density of accessible active sites remains a significant challenge, necessitating the development of synthesis methods that integrate multiple strategies. However, future research still needs to focus on these areas:

(1) Balancing activity and stability: In the design of non-precious metal single-atom catalysts, researchers have focused on enhancing activity by improving intrinsic activity and increasing active site density. However, balancing activity and stability remains a significant challenge. Recent studies suggest that combining non-precious and precious metals into clusters or ordered alloys can achieve high activity through synergistic effects while maintaining desirable stability. Although catalysts demonstrate ideal activity and stability in laboratory tests, their performance often degrades in PEMFC operations. This discrepancy necessitates a deeper understanding of catalyst degradation mechanisms under real-world conditions and further optimization of the MEA process to improve mass transfer, which is

critical for stability studies.

(2) Advanced characterization and theoretical insights: Characterization techniques, such as STEM and *in situ* TEM, have significantly advanced the understanding of single-atom catalyst structures. However, analyzing specific changes in active sites under operating conditions requires more advanced characterization methods. Theoretical calculations are also essential for designing and improving M-N-C catalysts. For example, earlier studies demonstrated that FeN_4 sites exhibit higher ORR activity than other FeN_x configurations. Recent theoretical studies, however, suggest that axially coordinated FeN_5 or FeN_2 sites have electronic structures more favorable for intermediate adsorption/desorption. These findings highlight the importance of theoretical calculations in catalyst design and underscore the value of integrating theoretical insights with advanced characterization techniques to accelerate the development of M-N-C catalysts.

(3) Scalability and cost-effectiveness: For non-precious metal ORR catalysts to become commercially viable, future research should focus on developing non-precious metal ORR catalysts that are scalable and cost-effective synthesis methods. Although base metal single-atom catalysts (SACs) theoretically exhibit the highest activity, practical synthesis methods remain limited. Incorporating small amounts of noble metals into SACs can leverage the activity of noble metals and the stability of non-platinum metals. However, ensuring the consistent quality and reliability of large-scale production faces challenges. Optimizing synthesis conditions and post-processing steps will be critical to producing catalysts at the gram or kilogram scale, which is critical for industrial applications.

Acknowledgements This work was supported by the National Natural Science Foundation of China (Grant No. 22379123), the High-level Innovation and Entrepreneurship Talent Project from Qinchuangyuan of Shaanxi Province (Grant No. QCYRCXM-2022-226), the Key Research and Development Program of Shaanxi Province (Grant No. 2024CY-GJHX-25), the National Natural Science Foundation of China, Pilot Group Program of the Research Fund for International Senior Scientists (Grant No.22250710676).

Competing Interests The authors declare no competing financial interest.

References

1. Mohideen M M, Radhamani A V, Ramakrishna S, et al. Recent insights on iron based nanostructured electrocatalyst and current status of proton exchange membrane fuel cell for sustainable transport. Journal of Energy Chemistry, 2022, 69: 466–489
2. Wang L, Wan X, Liu S, et al. Fe-N-C catalysts for PEMFC: Progress towards the commercial application under DOE reference. Journal of Energy Chemistry, 2019, 39: 77–87
3. Yuan Y, Zheng Y, Luo D, et al. Recent progress on mechanisms, principles, and strategies for high-activity and high-stability non-PGM fuel cell catalyst design. Carbon Energy, 2024, 6(5): e426
4. Wang Y, Chu T. Improvement of durability of membrane electrode assembly by frame sealing structure in temperature shock. Frontiers in Energy, early access, https://doi.org/10.1007/s11708–024-0955–3
5. Zaman S, Huang L, Douka A I, et al. Oxygen reduction electrocatalysts toward practical fuel cells: Progress and perspectives. Angewandte Chemie International Edition, 2021, 60(33): 17832–17852
6. Yuan C, Zhang S, Zhang J. Oxygen reduction electrocatalysis: From conventional to single-atomic platinum-based catalysts for proton exchange membrane fuel cells. Frontiers in Energy, 2024, 18(2): 206–222
7. Bae G, Kim M M, Han M H, et al. Unravelling the complex causality behind Fe-N-C degradation in fuel cells. Nature Catalysis, 2023, 6(12): 1140–1150
8. Fu X, Li N, Ren B, et al. Tailoring FeN_4 sites with edge enrichment for boosted oxygen reduction performance in proton exchange membrane fuel cell. Advanced Energy Materials, 2019, 9(11): 1803737
9. Delaporte N, Rivard E, Natarajan S K, et al. Synthesis and performance of MOF-based non-noble metal catalysts for the oxygen reduction reaction in proton-exchange membrane fuel cells: A review. Nanomaterials, 2020, 10(10): 1947
10. He Y, Guo H, Hwang S, et al. Single cobalt sites dispersed in hierarchically porous nanofiber networks for durable and high-power PGM-free cathodes in fuel cells. Advanced Materials, 2020, 32(46): 2003577
11. Wan K, Chu T, Li B, et al. Rational design of atomically dispersed metal site electrocatalysts for oxygen reduction reaction. Advanced Science, 2023, 10(11): 2203391
12. Sun M, Chen C, Wu M, et al. Rational design of Fe-N-C electrocatalysts for oxygen reduction reaction: From nanoparticles to single atoms. Nano Research, 2022, 15(3): 1753–1778
13. Hao Z, Ma Y, Chen Y, et al. Non-noble metal catalysts in cathodic oxygen reduction reaction of proton exchange membrane fuel cells: Recent advances. Nanomaterials, 2022, 12(19): 3331
14. Wang M, Zhang H, Liu Y, et al. Research progress of precise structural regulation of single atom catalyst for accelerating electrocatalytic oxygen reduction reaction. Journal of Energy Chemistry, 2022, 72: 56–72
15. Lin X, Peng P, Guo J, et al. A new steric tetra-imidazole for facile synthesis of high loading atomically dispersed FeN_4 electrocatalysts. Nano Energy, 2021, 80: 105533
16. Li J, Xia W, Tang J, et al. Metal-organic framework-derived graphene mesh: A robust scaffold for highly exposed Fe-N_4 active sites toward an excellent oxygen reduction catalyst in acid media. Journal of the American Chemical Society, 2022, 144(21): 9280–9291
17. Zhan Y, Zeng H, Zhao T, et al. Densely accessible single atom Fe sites dispersed on porous carbon as highly stable and active ORR catalyst for PEMFC. International Journal of Hydrogen

Energy, 2024, 56: 1049–1056
18. Hu C, Jin H, Liu B, et al. Propagating Fe-N_4 active sites with vitamin C to efficiently drive oxygen electrocatalysis. Nano Energy, 2021, 82: 105714
19. Chi B, Zhang L, Yang X, et al. Promoting ZIF-8-derived Fe-N-C oxygen reduction catalysts via Zr doping in proton exchange membrane fuel cells: Durability and Activity Enhancements. ACS Catalysis, 2023, 13(7): 4221–4230
20. Martinez U, Komini Babu S, Holby E F, et al. Progress in the development of Fe-based PGM-free electrocatalysts for the oxygen reduction reaction. Advanced Materials, 2019, 31(31): 1806545
21. Lin L, Fu C, Shen S, et al. Influence of Fe on electrocatalytic activity of iron-nitrogen-doped carbon materials toward oxygen reduction reaction. Frontiers in Energy, 2022, 16(5): 812-821
22. Kim J, Yoo J M, Lee H S, et al. Single-atom M-N-C catalysts for oxygen reduction electrocatalysis. Trends in Chemistry, 2021, 3(9): 779–794
23. Bhoyate S D, Kim J, de Souza F M, et al. Science and engineering for non-noble-metal-based electrocatalysts to boost their ORR performance: A critical review. Coordination Chemistry Reviews, 2023, 474: 214854
24. Wang Y, Hao J, Liu Y, et al. Recent advances in regulating the performance of acid oxygen reduction reaction on carbon-supported non-precious metal single atom catalysts. Journal of Energy Chemistry, 2023, 76: 601–616
25. Pang R, Xia H, Li J, et al. Recent developments of atomically dispersed metal electrocatalysts for oxygen reduction reaction. Chinese Journal of Chemistry, 2023, 41(5): 581–598
26. Wang D, Yang P, Liu L, et al. Atomically dispersed metal-nitrogen-carbon electrocatalysts for oxygen reduction reaction: from synthesis strategies to activity engineering. Materials Today. Energy, 2022, 26: 101017
27. Zhang P, Wang Y, You Y, et al. Generation pathway of hydroxyl radical in Fe/N/C-based oxygen reduction electrocatalysts under acidic media. Journal of Physical Chemistry Letters, 2021, 12(32): 7797–7803
28. Liu J, Jin Z, Wang X, et al. Recent advances in active sites identification and regulation of M-N/C electro-catalysts towards ORR. Science China. Chemistry, 2019, 62(6): 669–683
29. Zhang D, She F, Chen J, et al. Why do weak-binding M-N-C single-atom catalysts possess anomalously high oxygen reduction activity? Journal of the American Chemical Society, 2025, 147(7): 6076–6086
30. Li C, Zhao D H, Long H L, et al. Recent advances in carbonized non-noble metal-organic frameworks for electrochemical catalyst of oxygen reduction reaction. Rare Metals, 2021, 40(10): 2657–2689
31. Zhao Y, Wang Q, Hu R, et al. Oxygen reduction reaction performance of Fe-N-C catalyst with dual nitrogen source. Frontiers in Energy, 2024, 18(6): 841–849
32. Lu X, Yang P, Wan Y, et al. Active site engineering toward atomically dispersed M-N-C catalysts for oxygen reduction reaction. Coordination Chemistry Reviews, 2023, 495: 215400
33. Han A, Sun W, Wan X, et al. Construction of Co_4 atomic clusters to enable Fe-N_4 motifs with highly active and durable oxygen reduction performance. Angewandte Chemie International Edition, 2023, 62(30): e202303185
34. Wang X X, Cullen D A, Pan Y T, et al. Nitrogen-coordinated single cobalt atom catalysts for oxygen reduction in proton exchange membrane fuel cells. Advanced Materials, 2018, 30(11): 1706758
35. He Y, Shi Q, Shan W, et al. Dynamically unveiling metal-nitrogen coordination during thermal activation to design high-efficient atomically dispersed CoN_4 active sites. Angewandte Chemie International Edition, 2021, 60(17): 9516–9526
36. Zhang C, Zhang W, Zheng W. Transition metal-nitrogen-carbon active site for oxygen reduction electrocatalysis: Beyond the fascinations of TM-N_4. ChemCatChem, 20198, 11(2): 655–668
37. An Q, Bo S, Jiang J, et al. Atomic-level interface engineering for boosting oxygen electrocatalysis performance of single-atom catalysts: From metal active center to the first coordination sphere. Advanced Science, 2022. 10(4): 2205031
38. Kramm U I, Herranz J, Larouche N, et al. Structure of the catalytic sites in Fe/N/C-catalysts for O_2-reduction in PEM fuel cells. Physical Chemistry Chemical Physics, 2012, 14(33): 11673–11688
39. Yang X, Chen C, Zhou Z, et al. Advances in active site structure of carbon-based non-precious metal catalysts for oxygen reduction reaction. Acta Physico-Chimica Sinica, 2019, 35(5): 472–485 (in Chinese)
40. Li Y, Liu X, Zheng L, et al. Preparation of Fe-N-C catalysts with FeN_x (x = 1, 3, 4) active sites and comparison of their activities for the oxygen reduction reaction and performances in proton exchange membrane fuel cells. Journal of Materials Chemistry. A, Materials for Energy and Sustainability, 2019, 7(45): 26147–26153
41. Zhao C X, Li B Q, Liu J N, et al. Intrinsic electrocatalytic activity regulation of M-N-C single-atom catalysts for the oxygen reduction reaction. Angewandte Chemie International Edition, 2021, 60(9): 4448–4463
42. He Y, Liu S, Priest C, et al. Atomically dispersed metal-nitrogen-carbon catalysts for fuel cells: advances in catalyst design, electrode performance, and durability improvement. Chemical Society Reviews, 2020, 49(11): 3484–3524
43. Li L, Huang B, Tang X, et al. Recent developments of microenvironment engineering of single-atom catalysts for oxygen reduction toward desired activity and selectivity. Advanced Functional Materials, 2021, 31(45): 2103857
44. Ma R, Wang J, Tang Y, et al. Design strategies for single-atom iron electrocatalysts toward efficient oxygen reduction. Journal of Physical Chemistry Letters, 2022, 13(1): 168–174
45. Jiao L, Li J, Richard L L, et al. Chemical vapour deposition of Fe-N-C oxygen reduction catalysts with full utilization of dense Fe-N_4 sites. Nature Materials, 2021, 20(10): 1385–1391
46. Zhang X, Truong-Phuoc L, Asset T, et al. Are Fe-N-C electrocatalysts an alternative to Pt-based electrocatalysts for the next generation of proton exchange membrane fuel cells? ACS Catalysis, 2022, 12(22): 13853–13875
47. Wang X, Kang Z, Wang D, et al. Electronic structure regulation of the Fe-based single-atom catalysts for oxygen electrocatalysis. Nano Energy, 2024, 121: 109268

48. Yang Q, Jia Y, Wei F, et al. Understanding the activity of Co-$N_{4-x}C_x$ in atomic metal catalysts for oxygen reduction catalysis. Angewandte Chemie International Edition, 2020, 59(15): 6122–6127
49. Shen H, Gracia-Espino E, Ma J, et al. Atomically FeN_2 moieties dispersed on mesoporous carbon: A new atomic catalyst for efficient oxygen reduction catalysis. Nano Energy, 2017, 35: 9–16
50. Qi W, Zhang X, Niu J, et al. Mechanism insight into the oxygen reduction reaction on dual FeN_2 embedded graphene for proton exchange membrane fuel cells. Sustainable Energy & Fuels, 2022, 6(17): 4024–4033
51. Wang M, Wang L, Li Q, et al. Regulating the coordination geometry and oxidation state of single-atom Fe sites for enhanced oxygen reduction electrocatalysis. Small, 2023, 19(24): 2300373
52. Liu J, Gong Z, Allen C, et al. Edge-hosted Fe-N_3 sites on a multiscale porous carbon framework combining high intrinsic activity with efficient mass transport for oxygen reduction. Chem Catalysis, 2021, 1(6): 1291–1307
53. Yu L, Huang Q, Wu J, et al. Spatial-five coordination promotes the high efficiency of CoN_4 moiety in graphene-based bilayer for oxygen reduction electrocatalysis: A density functional theory study. Chinese Journal of Chemical Engineering, 2023, 54: 106–113
54. Nematollahi P, Barbiellini B, Bansil A, et al. Identification of a robust and durable FeN_4C_x catalyst for ORR in PEM fuel cells and the role of the fifth ligand. ACS Catalysis, 2022, 12(13): 7541–7549
55. Fu Y, Zhao Q, Wei Q, et al. Non-precious metal-based single-atom catalysts for oxygen reduction reaction: Fundamentals and applications. Materials Science and Engineering R Reports, 2024, 160: 100822
56. Liu F, Yan N, Zhu G, et al. Fe-N-C single-atom catalysts with an axial structure prepared by a new design and synthesis method for ORR. New Journal of Chemistry, 2021, 45(29): 13004–13014
57. Xia W, Hou Z, Tang J, et al. Materials informatics-guided superior electrocatalyst: A case of pyrolysis-free single-atom coordinated with N-graphene nanomesh. Nano Energy, 2022, 94: 106868
58. Zhang L, Meng Q, Zheng R, et al. Microenvironment regulation of M-N-C single-atom catalysts towards oxygen reduction reaction. Nano Research, 2023, 16(4): 4468–4487
59. Liu D, Wan X, Shui J. Tailoring oxygen reduction reaction on M-N-C catalysts via axial coordination engineering. Small, 2024, 20(50): e2406078
60. Zhao S H, Pan Y. Principles of coordination structure design of single-atom catalysts in electrocatalytic oxygen reduction reaction. Rare Metals, 2025
61. Li J, Zhang H, Samarakoon W, et al. Thermally driven structure and performance evolution of atomically dispersed FeN_4 sites for oxygen reduction. Angewandte Chemie International Edition, 2019, 58(52): 18971–18980
62. Wen X, Yu C, Yan B, et al. Morphological and microstructural engineering of Mn-N-C with strengthened Mn-N bond for efficient electrochemical oxygen reduction reaction. Chemical Engineering Journal, 2023, 475: 146135
63. Zha S, Wang D, Liu C, et al. Heteroatom doped M-N-C single-atom catalysts for high-efficiency oxygen reduction reaction: Regulation of coordination configurations. Sustainable Energy & Fuels, 2022, 6(17): 3895–3906
64. Xie X, Peng H, Ma G, et al. Recent progress in heteroatom doping to modulate the coordination environment of M-N-C catalysts for the oxygen reduction reaction. Materials Chemistry Frontiers, 2023, 7(13): 2595–2619
65. Wang Y, Chen Y, Wang Z, et al. Boron doping induced electronic reconfiguration of Fe-N_x sites in N-doped carbon matrix for efficient oxygen reduction reaction in both alkaline and acidic media. International Journal of Hydrogen Energy, 2022, 47(43): 18663–18674
66. Zhang J, Zhang J, He F, et al. Defect and doping Co-engineered non-metal nanocarbon ORR electrocatalyst. Nano-Micro Letters, 2021, 13(1): 65
67. Liu L L, Ma M X, Xu H, et al. S-doped M-N-C catalysts for the oxygen reduction reaction: Synthetic strategies, characterization, and mechanism. Journal of Electroanalytical Chemistry, 2022, 920: 116637
68. Wang Y C, Lai Y J, Song L, et al. S-doping of an Fe/N/C ORR catalyst for polymer electrolyte membrane fuel cells with high power density. Angewandte Chemie International Edition, 2015, 54(34): 9907–9910
69. Li P, Guo Q, Zhang J, et al. How the microenvironment dominated by the distance effect to regulate the FeN_4 site ORR activity and selectivity? Nano Research, 2024, 17(6): 5735–5741
70. Liu B, Li J, Yan B, et al. Sulfur doped iron-nitrogen-hard carbon nanosheets as efficient and robust noble metal-free catalysts for oxygen reduction reaction in PEMFC. Journal of Energy Chemistry, 2024, 89: 422–433
71. Sun T, Zang W, Yan H, et al. Engineering the coordination environment of single cobalt atoms for efficient oxygen reduction and hydrogen evolution reactions. ACS Catalysis, 2021, 11(8): 4498–4509
72. Roh J, Cho A, Kim S, et al. Transformation of the active moiety in phosphorus-doped Fe-N-C for highly efficient oxygen reduction reaction. ACS Catalysis, 2023, 13(14): 9427–9441
73. Li Y, Ren P, Lu X, et al. Elucidating the role of P on Mn- and N-doped graphene catalysts in promoting oxygen reduction: Density functional theory studies. SusMat, 2023, 3(3): 390–401
74. Yin H, Yuan P, Lu B A, et al. Phosphorus-driven electron delocalization on edge-type FeN_4 active sites for oxygen reduction in acid medium. ACS Catalysis, 2021, 11(20): 12754–12762
75. Xue W, Zhou Q, Cui X, et al. Atomically dispersed FeN_2P_2 motif with high activity and stability for oxygen reduction reaction over the entire pH range. Angewandte Chemie International Edition, 2023, 62(41): e202307504
76. Hsieh C T, Kao C P, Gandomi Y A, et al. Oxygen reduction reactions from boron-doped graphene quantum dot catalyst electrodes in acidic and alkaline electrolytes. Journal of the Taiwan Institute of Chemical Engineers, 2022, 133: 104196
77. Guo Y, Yuan P, Zhang J, et al. Carbon nanosheets containing

discrete Co-N_x-by-C active sites for efficient oxygen electrocatalysis and rechargeable Zn-air batteries. ACS Nano, 2018, 12(2): 1894–1901

78. Xin C, Shang W, Hu J, et al. Integration of morphology and electronic structure modulation on atomic iron-nitrogen-carbon catalysts for highly efficient oxygen reduction. Advanced Functional Materials, 2022, 32(2): 2108345
79. Hu L, Dai C, Chen L, et al. Metal-triazolate-framework-derived FeN_4C_{l1} single-atom catalysts with hierarchical porosity for the oxygen reduction reaction. Angewandte Chemie International Edition, 2021, 60(52): 27324–27329
80. Sun P, Qiao K, Li D, et al. Designing oxygen-doped Fe-N-C oxygen reduction catalysts for proton- and anion-exchange-membrane fuel cells. Chem Catalysis, 2022, 2(10): 2750–2763
81. Huo J, Cao X, Tian Y, et al. Atomically dispersed Mn atoms coordinated with N and O within an N-doped porous carbon framework for boosted oxygen reduction catalysis. Nanoscale, 2023, 15(11): 5448–5457
82. Kumar K, Dubau L, Jaouen F, et al. Review on the degradation mechanisms of metal-N-C catalysts for the oxygen reduction reaction in acid electrolyte: Current understanding and mitigation approaches. Chemical Reviews, 2023, 123(15): 9265–9326
83. Yan Y, Cheng H, Qu Z, et al. Recent progress on the synthesis and oxygen reduction applications of Fe-based single-atom and double-atom catalysts. Journal of Materials Chemistry. A, Materials for Energy and Sustainability, 2021, 9(35): 19489–19507
84. Cheng Y, Hu S, Luo G, et al. FeCoN Co-doped hollow carbon nanocage grafted with carbon nanotubes as an electrocatalyst for enhanced oxygen reduction reaction. ACS Applied Energy Materials, 2023, 6(3): 2010–2021
85. Pedersen A, Barrio J, Li A, et al. Dual-metal atom electrocatalysts: Theory, synthesis, characterization, and applications. Advanced Energy Materials, 2022, 12(3): 2102715
86. Tong M, Sun F, Xie Y, et al. Operando cooperated catalytic mechanism of atomically dispersed Cu-N_4 and Zn-N_4 for promoting oxygen reduction reaction. Angewandte Chemie International Edition, 2021, 60(25): 14005–14012
87. Xie Y, Chen X, Sun K, et al. Direct oxygen-oxygen cleavage through optimizing interatomic distances in dual single-atom electrocatalysts for efficient oxygen reduction reaction. Angewandte Chemie International Edition, 2023, 62(17): e202301833
88. Li R, Wang D. Understanding the structure-performance relationship of active sites at atomic scale. Nano Research, 2022, 15(8): 6888–6923
89. Han Y, Yin S, Chen Y, et al. Experimental and DFT studies of oxygen reduction reaction promoted by binary site Fe/Co-N-C catalyst in acid. Journal of Electroanalytical Chemistry, 2022, 914: 116322
90. Kong F, Wang M, Huang Y, et al. Cu-N-bridged Fe-3d electron state regulations for boosted oxygen reduction in flexible battery and PEMFC. Energy Storage Materials, 2023, 54: 533–542
91. Zhou Y, Yang W, Utetiwabo W, et al. Revealing of active sites and catalytic mechanism in N-coordinated Fe, Ni dual-doped carbon with superior acidic oxygen reduction than single-atom catalyst. Journal of Physical Chemistry Letters, 2020, 11(4): 1404–1410
92. Zhang X, Wang S, Xia Z, et al. Insights into (Mn/Fe/Co)M-N-C dual-atom catalysts for the oxygen reduction reaction: the critical role of structural evolution. New Journal of Chemistry, 2024, 48(45): 19241–19248
93. Wang Z, Jin X, Zhu C, et al. Atomically dispersed Co_2-N_6 and Fe-N_4 costructures boost oxygen reduction reaction in both alkaline and acidic media. Advanced Materials, 2021, 33(49): 2104718
94. Yang B, Yu H, Jia X, et al. Atomically dispersed isolated Fe-Ce dual-metal-site catalysts for proton-exchange membrane fuel cells. ACS Applied Materials & Interfaces, 2023, 15(19): 23316–23327
95. Liu Q, Cao S, Fu Y, et al. Trimetallic FeCoNi-N/C nanofibers with high electrocatalytic activity for oxygen reduction reaction in sulfuric acid solution. Journal of Electroanalytical Chemistry, 2018, 813: 52–57
96. Shao Y, Dodelet J P, Wu G, et al. PGM-free cathode catalysts for PEM fuel cells: A mini-review on stability challenges. Advanced Materials, 2019, 31(31): 1807615
97. Shen M, Wei C, Ai K, et al. Transition metal-nitrogen-carbon nanostructured catalysts for the oxygen reduction reaction: From mechanistic insights to structural optimization. Nano Research, 2017, 10(5): 1449–1470
98. Chen G, Lu R, Li C, et al. Hierarchically porous carbons with highly curved surfaces for hosting single metal FeN_4 sites as outstanding oxygen reduction catalysts. Advanced Materials, 2023, 35(32): 2300907
99. Li J, Xia W, Guo Y, et al. Surface curvature effect on single-atom sites for the oxygen reduction reaction: A model of mesoporous MOF-derived carbon. Chemical Engineering Journal, 2023, 477: 146841
100. Ma Q, Jin H, Zhu J, et al. Stabilizing Fe-N-C catalysts as model for oxygen reduction reaction. Advanced Science, 2021, 8(23): 2102209
101. Jiang S, Ye G, Zhu W, et al. Atomic Edge Fe-N_4 active sites on N-doped porous carbon nanosheets derived from zeolitic-imidazolate frameworks for high-efficiency oxygen reduction. ACS Sustainable Chemistry & Engineering, 2023, 11(48): 16926–16934
102. Kong F, Huang Y, Chen M, et al. Creation of densely exposed and cavity-edged single Fe active sites for enhanced oxygen electroreduction. Applied Catalysis B: Environmental, 2022, 317: 121768
103. Cui L, Zhao J, Liu G, et al. Rich edge-hosted single-atomic Cu-N_4 sites for highly efficient oxygen reduction reaction performance. Journal of Colloid and Interface Science, 2022, 622: 209–217
104. Noh W Y, Mun J, Lee Y, et al. Molecularly engineered carbon platform to anchor edge-hosted single-atomic M-N/C (M=Fe, Co, Ni, Cu) electrocatalysts of outstanding durability. ACS Catalysis, 2022, 12(13): 7994–8006
105. Zhang W, Han G, Liu C, et al. Unique electron-feeding mechanism in CoN_3O for enhanced acidic oxygen reduction.

Chemical Engineering Journal, 2024, 500: 156980
106. Kim K, Kim G, Jeong T, et al. Activating the Mn single atomic center for an efficient actual active site of the oxygen reduction reaction by spin-state regulation. Journal of the American Chemical Society, 2024, 146(49): 34033–34042
107. Li Y, Wu H R, Yu Y, et al. High-shell sulfur doping enhances Mn-N_4 spin states and boosts oxygen reduction reaction performance in both acidic and alkaline media. Small, 2025: 2411678
108. Huang G Y, Wang K A, Zhu G R, et al. Dual-atomic-sites anchored on nanosized hollow polyhedron to boost oxygen reduction reaction in acidic electrolyte. Journal of Power Sources, 2024, 592: 233970
109. Zhang P, Sun T, Jiang R, et al. A robust asymmetric diatomic electrocatalyst for oxygen reduction reaction in both acidic and alkaline media. Applied Catalysis B: Environmental, 2024, 344: 123645
110. Li Y, Luo X, Wei Z, et al. Precisely constructing charge-asymmetric dual-atom Fe sites supported on hollow porous carbon spheres for efficient oxygen reduction. Energy & Environmental Science, 2024, 17(13): 4646–4657
111. Yu Y, Wang Y, Yang F, et al. Meso/microporous single-atom catalysts featuring curved Fe-N_4 sites boost the oxygen reduction reaction activity. Angewandte Chemie International Edition, 2024, 64(3): e202415691
112. Liu B, Guo P, Dai Y, et al. Tailoring asymmetric atomic strain of FeN_4 sites for enhanced acidic oxygen reduction reaction. Chemical Engineering Journal, 2025, 507: 160174
113. He Y, Wu G. PGM-free oxygen-reduction catalyst development for proton-exchange membrane fuel cells: Challenges, solutions, and promises. Accounts of Materials Research, 2022, 3(2): 224–236
114. Li Y, Qiao L, Yin S, et al. A plasma-assisted approach to enhance density of accessible FeN_4 sites for proton exchange membrane fuel cells. Journal of Colloid and Interface Science, 2023, 647: 224–232
115. Osmieri L, Meyer Q. Recent advances in integrating platinum group metal-free catalysts in proton exchange membrane fuel cells. Current Opinion in Electrochemistry, 2022, 31: 100847
116. Wan X, Chen W, Yang J, et al. Synthesis and active site identification of Fe-N-C single-atom catalysts for the oxygen reduction reaction. ChemElectroChem, 2019, 6(2): 304–315
117. Sarapuu A, Lilloja J, Akula S, et al. Recent advances in non-precious metal single-atom electrocatalysts for oxygen reduction reaction in low-temperature polymer-electrolyte fuel cells. ChemCatChem, 2023, 15(22): e202300849
118. Wang X, Zhang L, Xiao M, et al. Polymer-chelation approach to high-performance Fe-N_x-C catalyst towards oxygen reduction reaction. Chinese Chemical Letters, 2023, 34(4): 107455
119. Zhang B, Guo H, Zhang L, et al. Carbon composites from iron-chelating pyridine nitrogen-rich coordinated nanosheets for oxygen reduction. Functional Composite Materials, 2022, 3(1): 2
120. Xu L, Wang P, Wu S. Chelation-assisted synthesis of chitosan-derived Mn-N-C electrocatalyst for efficient oxygen reduction reaction. Inorganic Chemistry Communications, 2023, 156: 111227
121. Xia C, Qiu Y, Xia Y, et al. General synthesis of single-atom catalysts with high metal loading using graphene quantum dots. Nature Chemistry, 2021, 13(9): 887–894
122. Wang K, Chai H, Cao Y. Using anion-exchange to induce the formation of edge defects in CoN_x to enhance ORR activity. ChemCatChem, 2022, 14(13): e202200146
123. Jiang R, Qiao Z, Xu H, et al. Defect engineering of Fe-N-C single-atom catalysts for oxygen reduction reaction. Chinese Journal of Catalysis, 2023, 48: 224–234
124. Yi S Y, Choi E, Jang H Y, et al. Insight into defect engineering of atomically dispersed iron electrocatalysts for high-performance proton exchange membrane fuel cell. Advanced Materials, 2023, 35(46): 2302666
125. Yao X, Zhu Y, Xia T, et al. Tuning carbon defect in copper single-atom catalysts for efficient oxygen reduction. Small, 2023, 19(28): 2301075
126. Yang Z, Wang X, Zhu M, et al. Structural revolution of atomically dispersed Mn sites dictates oxygen reduction performance. Nano Research, 2021, 14(12): 4512–4519
127. Zhao Y, Chen H C, Ma X, et al. Vacancy defects inductive effect of asymmetrically coordinated single-atom Fe-N_3S_1 active sites for robust electrocatalytic oxygen reduction with high turnover frequency and mass activity. Advanced Materials, 2024, 36(11): 2308243
128. Tang T, Ding L, Jiang Z, et al. Advanced transition metal/nitrogen/carbon-based electrocatalysts for fuel cell applications. Science China. Chemistry, 2020, 63(11): 1517–1542
129. Zhao L, Zhang Y, Huang L B, et al. Cascade anchoring strategy for general mass production of high-loading single-atomic metal-nitrogen catalysts. Nature Communications, 2019, 10(1): 1278
130. Du Q, Zhu C, Yue C, et al. Anchoring atomically dispersed FeN_5 sites on porous and defect-rich biochar via cascade regulation strategy for efficient Fenton-like catalysis. Applied Catalysis B: Environmental, 2024, 343: 123570
131. Hai X, Xi S, Mitchell S, et al. Scalable two-step annealing method for preparing ultra-high-density single-atom catalyst libraries. Nature Nanotechnology, 2021, 17(2): 174–181.
132. Zhou Z, Fang H, Liu Y, et al. ZIF-8-derived dual metal (Fe, Ni)-nitrogen-doped porous carbon for superior ORR performance in universal acid-base properties solutions. Israel Journal of Chemistry, 2023, 63(12): e202200058
133. Gao C, Mu S, Yan R, et al. Recent advances in ZIF-derived atomic metal-N-C electrocatalysts for oxygen reduction reaction: Synthetic strategies, active centers, and stabilities. Small, 2022, 18(14): 2105409
134. Cai N, Fu L, Yang Z, et al. Innovative strategies to effectively increase the active-site density of M-N-C materials for electrochemical application. Current Opinion in Electrochemistry, 2022, 34: 100994
135. Yu J, Su C, Shang L, et al. Single-atom-based oxygen reduction reaction catalysts for proton exchange membrane fuel cells: Progress and Perspective. ACS Nano, 2023, 17(20): 19514–19525
136. Chen Y, Ji S, Wang Y, et al. Isolated single iron atoms anchored

on N-doped porous carbon as an efficient electrocatalyst for the oxygen reduction reaction. Angewandte Chemie International Edition, 2017, 56(24): 6937–6941

137. Yang X, Li X, Liu M, et al. Confined synthesis of dual-atoms within pores of covalent organic frameworks for oxygen reduction reaction. Small, 2024, 20(14): 2306295
138. Liu M, Liu J, Song Y, et al. Mononuclear iron-dependent electrocatalytic activity of metal-nitrogen-carbon catalysts for efficient oxygen reduction reaction. Applied Catalysis A, General, 2019, 583: 117120
139. Deng L, Qiu L, Hu R, et al. Restricted diffusion preparation of fully-exposed Fe single-atom catalyst on carbon nanospheres for efficient oxygen reduction reaction. Applied Catalysis B: Environmental, 2022, 305: 121058
140. Gu M X, Gao L P, Peng S S, et al. Transitionmetal single atoms constructed by using inherent confined space. ACS Nano, 2023, 17(5): 5025–5032
141. Mukherjee P, Saravanan P. Pyrolytically synthesized cobalt based carbon nitrogen framework as an efficient cathode catalyst in MFC application. Journal of Environmental Chemical Engineering, 2022, 10(6): 108940
142. Zhou Y, Tao X, Chen G, et al. Multilayer stabilization for fabricating high-loading single-atom catalysts. Nature Communications, 2020, 11(1): 5892
143. Li L, Zhang L, Xu Z, et al. Hierarchically porous carbons fabricated by dual pore-forming approach for the oxygen reduction reaction. Carbon, 2022, 189: 634–641
144. Wang R, Yang Y, Zhao Y, et al. Multiscale structural engineering of atomically dispersed FeN4 electrocatalyst for proton exchange membrane fuel cells. Journal of Energy Chemistry, 2021, 58: 629–635
145. Akula S, Mooste M, Kozlova J, et al. Transition metal (Fe, Co, Mn, Cu) containing nitrogen-doped porous carbon as efficient oxygen reduction electrocatalysts for anion exchange membrane fuel cells. Chemical Engineering Journal, 2023, 458: 141468
146. Kiciński W, Dyjak S, Gratzke M, et al. Platinum group metal-free Fe-N-C catalysts for PEM fuel cells derived from nitrogen and sulfur doped synthetic polymers. Fuel, 2022, 328: 125323
147. Jiao L, Arman T A, Hwang S, et al. Self-sacrificial template synthesis of Fe-N-C catalysts with dense active sites deposited on a porous carbon network for high performance in PEMFC. Advanced Energy Materials, 2024, 14(20): 2303952
148. Tan H, Tang J, Kim J, et al. Rational design and construction of nanoporous iron- and nitrogen-doped carbon electrocatalysts for oxygen reduction reaction. Journal of Materials Chemistry. A, Materials for Energy and Sustainability, 2019, 7(4): 1380–1393
149. Akula S, Mooste M, Zulevi B, et al. Mesoporous textured Fe-N-C electrocatalysts as highly efficient cathodes for proton exchange membrane fuel cells. Journal of Power Sources, 2022, 520: 230819
150. Rao X, Zhang S, Zhang J. Effectively controlling the nanostructures and active sites of non-noble carbon catalysts for improving oxygen reduction reaction. Current Opinion in Electrochemistry, 2023, 42: 101416
151. Wang Q, Yang Y, Sun F, et al. Molten NaCl-assisted synthesis of porous Fe-N-C electrocatalysts with a high density of catalytically accessible FeN_4 active sites and outstanding oxygen reduction reaction performance. Advanced Energy Materials, 2021, 11(19): 2100219
152. Hao J, Wang Y, Qiu X, et al. Dual inorganic sacrificial template synthesis of hierarchically porous carbon with specific N sites for efficient oxygen reduction. ACS Applied Materials & Interfaces, 2021, 13(24): 28140–28149
153. Miao W, Huang F, Shen X, et al. Single atom Fe-based catalyst derived from hierarchical (Fe,N)-ZIF-8/CNFs for high-efficient ORR activity. Materials Chemistry Frontiers, 2022, 6(21): 3213–3224
154. Jaramillo D, Alvarez G, Díaz C, et al. Porous carbonaceous materials simultaneously dispersing N, Fe and Co as bifunctional catalysts for the ORR and OER: electrochemical performance in a prototype of a Zn-air battery. Dalton Transactions, 2024, 53(7): 3143–3158
155. Lu X, Xu H, Yang P, et al. Zinc-assisted MgO template synthesis of porous carbon-supported Fe-Nx sites for efficient oxygen reduction reaction catalysis in Zn-air batteries. Applied Catalysis B: Environmental, 2022, 313: 121454
156. Sun F, Liu T, Huang M, et al. High specific surface area Fe-N-C electrocatalysts for the oxygen reduction reaction synthesized by a hard-template-assisted ball milling strategy. Sustainable Energy & Fuels, 2023, 7(15): 3675–3683
157. Sun J, Jin J, Chang Y, et al. Unravelling temperature ramping rates in fabricating NaCl-induced porous Co/N-C electrocatalysts for oxygen reduction reaction. ChemElectroChem, 2022, 9(11): e202200375
158. Niu W J, Li R J, Zhao W W, et al. Hierarchical porous Fe-N/C@surfactant composites synthesized by a surfactant-assisted strategy as high-performance bifunctional oxygen electrodes for rechargeable zinc-air batteries. Journal of Colloid and Interface Science, 2023, 649: 435–444
159. Zheng R, Meng Q, Zhang H, et al. Atomically dispersed Fe sites on hierarchically porous carbon nanoplates for oxygen reduction reaction. Journal of Energy Chemistry, 2024, 90: 7–15
160. Ma F X, Liu Z Q, Zhang G, et al. Isolating Fe atoms in N-doped carbon hollow nanorods through a ZIF-phase-transition strategy for efficient oxygen reduction. Small, 2022, 18(49): 2205033
161. Li J, Chen M, Cullen D A, et al. Atomically dispersed manganese catalysts for oxygen reduction in proton-exchange membrane fuel cells. Nature Catalysis, 2018, 1(12): 935–945
162. Guo L, Hu Y, Zhao X, et al. Secondary doping of Mn/Co bimetallic ZIF-derived catalysts for the oxygen reduction reaction. New Journal of Chemistry, 2023, 47(26): 12123–12132
163. Qu X, Li Y, Li G, et al. Boosting the ORR performance of Fe-N/C catalyst via increasing the density and modifying the electronic structure of Fe-N_x active sites. Electrochimica Acta, 2022, 403: 139604